MDPI

Review

Enrichment Characteristics and Mechanisms of Critical Metals in Marine Fe-Mn Crusts and Nodules: A Review

Sucheng Huang [1,2] and Yazhou Fu [1,*]

[1] State Key Laboratory of Ore Deposit Geochemistry, Institute of Geochemistry, Chinese Academy of Sciences, Guiyang 550081, China; huangsucheng@mail.gyig.ac.cn
[2] College of Earth and Planetary Sciences, University of Chinese Academy of Sciences, Beijing 100049, China
[*] Correspondence: fuyazhou@mail.gyig.ac.cn

Abstract: Marine Co-rich ferromanganese crusts and polymetallic nodules, which are widely distributed in oceanic environments, are salient potential mineral resources that are enriched with many critical metals. Many investigations have achieved essential progress and findings regarding critical metal enrichment in Fe-Mn crusts and nodules. This study systematically reviews the research findings of previous investigations and elaborates in detail on the enrichment characteristics, enrichment processes and mechanisms and the influencing factors of the critical metals enriched in Fe-Mn crusts and nodules. The influencing factors of critical metal enrichments in Fe-Mn crusts and nodules mainly include the growth rate, water depth, post-depositional phosphatization and structural uptake of adsorbents. The major enrichment pathways of critical metals in marine Fe-Mn (oxy)hydroxides are primarily as follows: direct substitution on the surface of δ-MnO_2 for Ni, Cu, Zn and Li; oxidative substitution on the δ-MnO_2 surface for Co, Ce and Tl; partition between Mn and Fe phases through surface complexation according to electro-species attractiveness for REY (except for Ce), Cd, Mo, W and V; combined Mn-Fe phases enrichment for seawater anionic Te, Pt, As and Sb, whose low-valence species are mostly oxidatively enriched on δ-MnO_2, in addition to electro-chemical adsorption onto FeOOH, while high-valence species are likely structurally incorporated by amorphous FeOOH; and dominant sorption and incorporation by amorphous FeOOH for Ti and Se. The coordination preferences of critical metals in the layered and tunneled Mn oxides are primarily as follows: metal incorporations in the layer/tunnel-wall for Co, Ni and Cu; triple-corner-sharing configurations above the structural vacancy for Co, Ni, Cu, Zn and Tl; double-corner-sharing configurations for As, Sb, Mo, W, V and Te; edge-sharing configurations at the layer rims for corner-sharing metals when they are less competitive in taking up the corner-sharing position or under less oxidizing conditions when the metals are less feasible for reactions with layer vacancy; and hydrated interlayer or tunnel-center sorption for Ni, Cu, Zn, Cd, Tl and Li. The major ore-forming elements (e.g., Co, Ni, Cu and Zn), rare earth elements and yttrium, platinum-group elements, dispersed elements (e.g., Te, Tl, Se and Cd) and other enriched critical metals (e.g., Li, Ti and Mo) in polymetallic nodules and Co-rich Fe-Mn crusts of different geneses have unique and varied enrichment characteristics, metal occurrence states, enrichment processes and enrichment mechanisms. This review helps to deepen the understanding of the geochemical behaviors of critical metals in oceanic environments, and it also bears significance for understanding the extreme enrichment and mineralization of deep-sea critical metals.

Keywords: cobalt-rich ferromanganese crusts; polymetallic nodules; critical metals; enrichment process; enrichment mechanism

1. Introduction

Marine ferromanganese (Fe-Mn) nodules and crusts, widely known as cobalt-rich Fe-Mn crusts and polymetallic nodules, are authigenic precipitates ubiquitously found on the vast oceanic abyssal plains and seamount flanks and plateaus [1–3]. They primarily form in two ways: hydrogenetic precipitation and diagenetic formation. Fe-Mn crusts and nodules

can form via hydrogenetic precipitation directly from ambient oxygen-rich seawater that contains abundant colloidal metals [3–5]. Fe-Mn nodules can also form through diagenetic processes occurring within suboxic pelagic sediments and porewater space, where abundant dissolved metal particles can emerge from microbial oxidation [2,5,6]. Aside from them, there are also hydrothermal crusts distributed in the ocean. Hydrogenetic and diagenetic crusts and nodules have a slow growth rate, as low as 1–10 mm/Ma, which provides sufficient durations for metal enrichments; they also have the unique physical properties of low bulk density (mean of 1.3 g/cm^3 dry bulk), large specific surface area (mean of 325 m^2 g^{-1}) and high porosity (mean of 60%) [2,3,7–9]. Fe-Mn nodules and crusts show dominant mineralogical compositions of vernadite, birnessite, buserite, asbolan, todorokite and amorphous Fe oxyhydroxides [5,10–12]. They are considered representative oceanic Fe-Mn minerals that exhibit abundant interlayers, tunnels and layers, with many vacancies for the incorporation of high amounts of metals [13–16]. These properties collectively make marine nodules and crusts some of the most effective metal scavengers in seawater that enrich large amounts of critical elements.

Critical metals are strategic metal resources that play crucial roles in modern development and green and advanced technology, e.g., solar cells (Te) and rechargeable batteries (Co); the criteria of critical metals have been attributed to rareness, high-tech applications and stable supply proficiency [17–19]. Marine Fe-Mn nodules and crusts have attracted scientific and economic attention because they can enrich significant amounts and tonnages of critical metals, such as cobalt [15,20], nickel [21,22] and rare earth elements and yttrium (REY) [23–25]. Figure 1 shows the critical metal enrichment levels in hydrogenetic crusts in the Pacific Prime Crust Zone (PCZ), hydrogenetic–diagenetic nodules in the Clarion–Clipperton Zone (CCZ) and diagenetic nodules from the Peru Basin. Their exceptional enrichments significantly exceed their respective abundances in the Earth's crust [2,4,26], PCZ Fe-Mn crusts have shown average Co, Mo and Tl concentrations of more than 100 times compared to the Earth's crust, while Te enrichment in Fe-Mn crusts can be as high as 50,000 times compared to the Earth's crust [26]. Co could exhibit high contents of more than 1% in hydrogenetic crusts [9], whereas Ni contents could easily reach up to more than 2% in CCZ nodules [6]. Previous findings showed that the enormous metal resources in marine Fe-Mn crusts and nodules greatly surpass those in land-based reserves [27–30]. For example, Co exhibits a large abundance of 42×10^6 and 50×10^6 tons in the Clarion–Clipperton Zone and Pacific Prime Crust Zone, which far exceed the land-based Co reserves of 8.3×10^6 tons, while more than 120 million tons of Co, Ni and REY resources have been identified in nodules and crusts [27–30]. The metal resources of Y, Tl and Te in Fe-Mn crusts also surpass their land-based reserves [20,28,31]. Thus, marine Fe-Mn crusts and nodules show promising potential to provide sustainable critical metal supplies.

The highly enriched critical metals, like Co, Ni, Cu, REY and platinum-group elements (PGEs), in marine Fe-Mn crusts and nodules have been vastly investigated for decades, achieving progressive findings, especially in research on their elemental occurrence states [32,33], sorption process [21,24] and enrichment mechanisms [15,20,31]. Additionally, Li, Te, Mo, W, V, As and Sb were also investigated due to their enrichment characteristics and enrichment processes and mechanisms [34–38]. A detailed discussion of their enrichments is presented in Section 5. However, there are still many unknowns and conflicts remaining regarding the critical metal occurrence states and enrichment mechanisms, which require further works. The latest review studies have elaborated on mineralogical compositions and resource potential [39–41], while some review studies also contributed to their detailed formation process and the chemical process of metal enrichment from a more general perspective [2–5,42]. Review studies also documented the exterior factors, such as water depth, longitude/latitude and ocean productivity [43,44]. However, there is only a very limited conclusive elaboration on the enrichment processes and mechanisms of the critical metals enriched in marine Fe-Mn deposits. In this study, we systematically discuss the critical metals enriched in marine Fe-Mn crusts and nodules,

analyze the effect of influencing factors on metal uptake and categorize major enrichment pathways and coordination preference for critical metals. We also individually elaborate on the enrichment behaviors, characteristics, micro-uptake process and mechanism of five groups of enriched critical metals based on a conclusive view of previous investigations. In our study of crusts and nodules, we mainly focus on Fe-Mn (oxy)hydroxides of hydrogenetic and diagenetic origins instead of hydrothermal origin. Typical hydrothermal crusts and nodules from various regions are exceptionally low in concentrations of many critical metals, e.g., Co, Ni [35,45] and REY [46–48], compared to typical hydrogenetic Pacific crusts and hydrogenetic–diagenetic CCZ nodules, usually no higher than 200 ppm. Despite the unique occurrence of hydrothermal Fe-Mn deposits containing high Co+Ni concentrations in Wallis and Futuna Islands [49], they only represent a unique study case. Hydrothermal deposits are also low in tonnage resources, they "play little economic role in modern marine systems" [5] and they are also not ubiquitous compared to hydrogenetic crusts and hydrogenetic–diagenetic nodules. This study also emphasizes that hydrogenetic nodules and hydrogenetic crusts share similarities in mineralogical and chemical compositions; they possess the same genesis and often show similar processes in adsorbing metals from seawater [2,33]. Therefore, this study discusses the enrichment mechanism of hydrogenetic nodules and hydrogenetic crusts in a collective manner. Diagenetic nodules, hydrogenetic–diagenetic nodules and phosphatized crusts that grow in different geneses, geological backgrounds and environments are separately discussed.
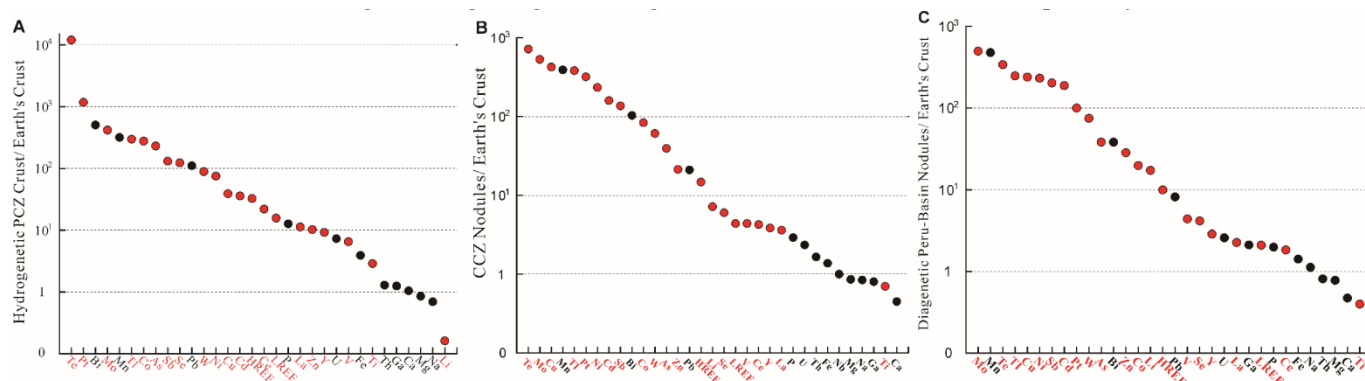

Figure 1. Compositions of representative hydrogenetic, hydrogenetic–diagenetic and diagenetic regions of marine Fe-Mn crusts and nodules, (**A**) Pacific Prime Crust Zone crusts, (**B**) Clarion–Clipperton Zone nodules, (**C**) Peru Basin nodules normalized to their respective contents in the Earth's crust. Critical metals discussed in this study are in red. Calculated from the data of [2,42,50].

2. Classification of Critical Metals

The identification of critical metals is not simply based on the metal's scarcity, previous critical metal lists shared similar criteria in defining critical metals [51,52]: (1) metals essential to economic prosperity, social security and stability; (2) metals capable of causing vulnerabilities to productions should their supply chains be disrupted; (3) metals that serve critical roles in advanced manufacturing, domestic productions and green/high-tech applications, the logistical disruptions of which would cause dire consequences on the economy and society [18,19,53]. China, the United States and the European Union, as the largest critical metal exporters and importers, share high similarities in their critical metal lists. Maintaining the stable supplies of critical metals and the acquisitions of critical metals are quickly becoming shared obstacles and norms for many countries [19,51,52]. The supplies of many critical metals (e.g., Co, REY and Li) among major countries heavily rely on imports, therefore substantiating continuous competition in resources and raw materials [17,54,55].

In this review study, we emphasize the strategic critical metals that are highly enriched in marine Fe-Mn crusts and nodules for elucidation (Table 1). We aim to discuss the enrichment characteristics and mechanisms of five groups of the publicly acknowledged

critical metals enriched in marine Fe-Mn crusts and nodules [5,17,18,26], which are as follows: (1) major ore-forming elements, Co, Ni, Cu and Zn; (2) rare earth elements and yttrium; (3) platinum group elements; (4) Te, Tl, Se and Cd of dispersed elements (dispersed elements refer to eight elements that are scatteringly distributed in the Earth's crust (usually in the order of 10^{-9}–10^{-6}) and hardly form independent ore deposits, which are Ga, Ge, Se, Cd, In, Te, Re and Tl) [56,57]; (5) other adequately enriched metals, which are Li, Ti, As, Sb, W, Mo and V. In addition, we note that some critical elements (e.g., Bi and U) that are also enriched to certain levels in marine Fe-Mn deposits have been excluded from the discussion due to their lack of relevant works and sufficient studies in the current research status.

Table 1. Critical metal compositions of representative Fe-Mn crusts and nodules areas of hydrogenetic, mixed and diagenetic genesis. PCZ: Pacific Prime Crust Zone. CCZ: Clarion–Clipperton Zone. PB: Peru Basin. The Peru Basin data are for a diagenetic nodule standard prepared by Bundesanstalt fur Geowissenschaffen und Rohstoffe (BGR), Germany of a large but unknown number of nodules; analyzed by the authors and presented here. The table is modified from [2,42].

Element	PCZ		CCZ		PB	
	Mean	**N**	**Mean**	**N**	**Mean**	**N**
Mn (wt.%)	22.8	362	28.1	54	34.2	-
Fe	16.9	362	5.92	54	6.12	-
Co (ppm)	6662	362	2011	54	475	-
Ni	4209	362	13,159	54	13,008	-
Cu	976	362	10,631	54	5988	-
Zn	668	325	1385	54	1845	-
Ce	1322	83	255	54	110	-
La	272	83	108	54	68	-
Y	221	294	92	54	69	-
LREE	2044.3	83	570.53	54	272.97	-
HREE	425.23	83	191.57	54	129.54	-
Li	2.92	33	129	54	311	-
Te	60	43	3.6	54	1.7	-
Cd	3.59	285	16	12	18.8	-
Se	14.8	1	0.72	12	0.5	-
Tl	155	34	199	12	129	-
As	393	328	67	12	65	-
Sb	39.3	43	41	12	61	-
V	641	328	429	54	431	-
W	89	36	61	54	75	-
Mo	461	328	587	54	547	-
Ti	11,600	345	2800	54	1600	-
Pt (ppb)	470	60	128	12	40	-

3. Influencing Factors of Critical Metal Uptake

The elemental uptakes in Fe-Mn crusts and nodules and their formation are highly influenced by a series of chemical interactions and exterior factors. This segment aims at describing the influences of the electro-chemical preferences of metal speciation, seawater depths, the growth rates of ferromanganese crusts and nodules, post-depositional phosphatization and the micro-structures of the Fe-Mn adsorbents that collectively determine the metal adsorption capacities and metal enrichments [7,32,44,58].

3.1. Electro-Charge Preference

Metals in Fe-Mn crusts and nodules are mostly phase-related and controlled by elemental complexations that originate their electro-affinities to binding phases. For most metals enriched in marine Fe-Mn deposits, a dominance in Mn-phase or Fe-phase sorption preference can be observed [31–33,59]. δ-MnO$_2$ and amorphous FeOOH in Fe-Mn crusts and nodules each exhibit pH zero point charge (pH$_{zpc}$) of 2.8 and 8.5, indicating different electro-charged δ-MnO$_2$ and FeOOH surfaces at a modern seawater pH of 8

and exhibit attractiveness to positive and negative metal species in seawater as shown in electro-chemical preferences (Figure 2). Free cations and weak chloro-complexes like Co^{2+}, Ni^{2+}, $ZnCl^+$ and positive light rare earth elements (LREEs) in seawater are significantly attracted to negatively charged δ-MnO_2 particles, while oxyanion complexes like Mo, Te and heavy rare earth elements (HREEs) are attracted to slight positively charged amorphous FeOOH [32,33,60]. Binding preferences have been suggested to direct the metal enrichment process through the coulombic interactions and chemical exchanges [32]. However, further investigations also suggested that other factors could pose more prominent controls than the electron positivity (e.g., investigations on Pt and W have revealed that negatively charged species were enriched on the Mn phase through overcoming the electrostatic repulsion) [31,37,61]. Many sorption and co-precipitation experiments have applied synthesized goethite/ferrihydrite and hexagonal birnessite to simulate sorption behaviors of marine Fe-Mn (oxy)hydroxides [62–64]. They are considered ideal and ordered mineral variations of the natural Fe-Mn crust and nodule samples but their pH_{zpc} are slightly different and may cause sorption variations. Previous sequential leaching has yielded great implications on the elemental host phases and examination of the elemental electro-preferences, although the results of some complicated metals may show different host phases in in-situ observations, possibly due to readsorptions and other variables [31–33].
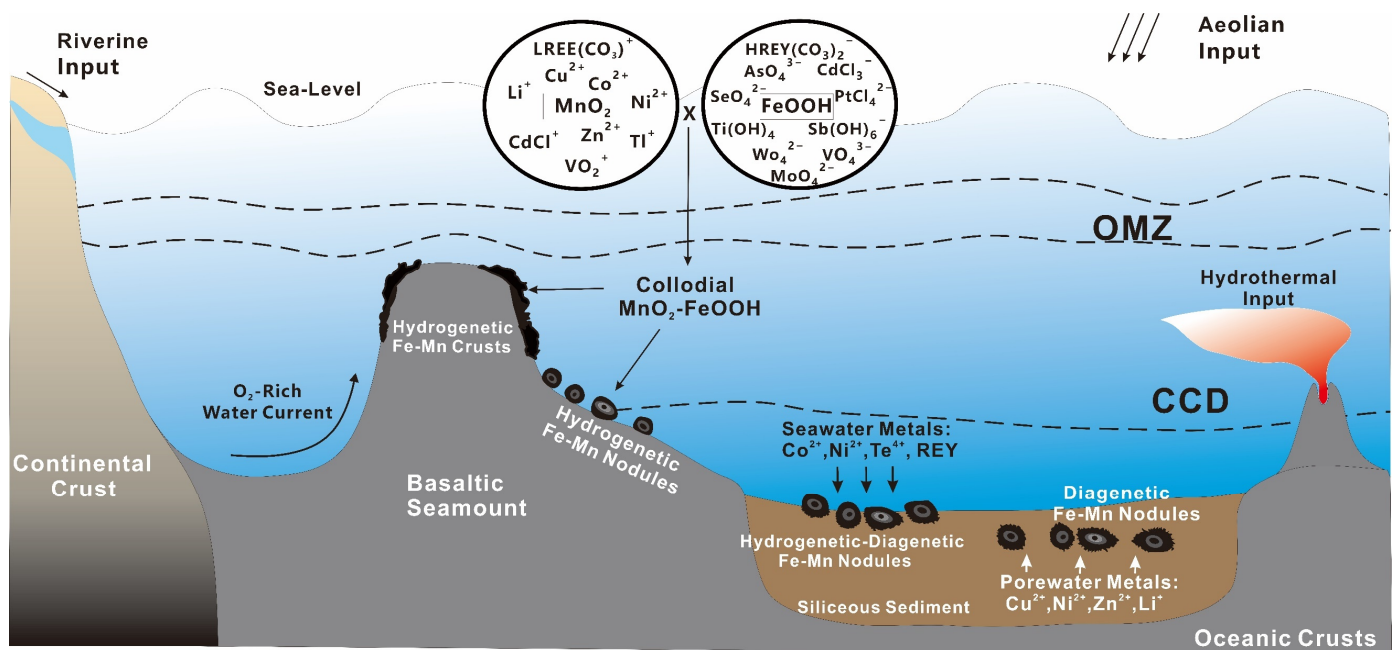

Figure 2. Schematic presentation showing the geneses, precipitation depths and locations of oceanic Fe-Mn crusts and nodules, electro-chemical model of sorption preferences on negatively charged Mn oxides and slightly positively charged Fe oxyhydroxides, OMZ: Oxygen Minimum Zone, CCD: Carbonate Compensation Depth. The graph is modified from [40].

3.2. Growth Rate

The growth rates of marine Fe-Mn crusts and nodules highly influence their metallic contents [43,65]. The growth rate is associated with mineral genesis, hydrogenetic growth is as low as 1–10 mm/Ma, whereas seafloor sediment-covered diagenetic growth with pore-water material contribution is 2–50 times faster [2,4,65,66]. In a typical seawater environment, the ultraslow growth rate allows Fe-Mn oxides to scavenge critical metals more abundantly from seawater, which provides sufficient durations for metal scavenging and further substantiates the high metal capacities of the hydrogenetic Fe-Mn oxides, typically for the scavenging-type elements and especially for Co and Ce that showed highly negative relations to the growth rates [9,20,67,68]. The low seawater concentrations of Co and Ce are compensated by the ultraslow growth rates [24,68,69]. It is noteworthy that Co

arguably shows the greatest sensitivity to the growth rate in hydrogenetic crust, which is manifested through its highly negative correlation to the growth rate and its application in calculating the growth rate [68,70,71]. Nodules and crusts with elevated growth rates typically show higher Ni+Cu and other elements rich in marine sediments and show lower concentrations of seawater-derived metals [6,14,44,65,71]. Thus, the variability of the growth rates could lead to content changes in metal abundance, which rationalizes the high abundances of correlated critical metals in crusts and nodules [7,40,68,71,72]. Some regions near lands or Fe-Mn crusts and nodules residing in the marginal seas, e.g., the California continental margin and the South China Sea, may have elevated growth rates contributed from terrestrial material inputs and relatively low Mn-related element abundances compared to the deep-sea Fe-Mn deposits [44,73,74]. However, some regions (e.g., the Sea of Okhotsk) do not seem to exhibit this trait [75]. Thus, the growth rate is related to Fe-Mn mineral genesis and could influence critical metal contents. Seawater-derived Co, Ce, Ti, Pt and REY that reveal a negative correlation with the growth rate are progressively accumulated in the low-growth-rate environments, whereas elements like Mo, W, V and Tl are less influenced, and elements like Li, Cu and Ni exhibit relatively higher concentrations with higher growth rates [29,47,76–79]. We note that the growth rate poses an influence on the metal concentration but does not decisively control the growth and the metal concentration of Fe-Mn crusts and nodules, for instance, Fe-Mn crusts in the North and Tropical Pacific have similar growth rates, but they vary in metal concentrations [80,81]. Other evident factors could also cause this variation, e.g., the effects of latitudes and oceanic productivity [43,44].

3.3. Water Depth

Depth variation exhibits a strong influence on the growth of marine Fe-Mn crusts and nodules and their metal abundances [43,58,82]. The oceanic-productivity-related O_2 minimum zone (OMZ) and carbonate compensation depth (CCD) release metallic colloids and materials for crust and nodule formation [7,44,83,84]. Ideal crusts usually precipitate just below the OMZ column and for nodules just below the CCD where oxic environments induced by the oxygen-rich ocean currents and the bountiful release of growth materials can be observed (Figure 2) [7]. Typical crusts precipitate at a water depth range of 400–4000 m, whereas nodules can be found deeper below the CCD on the vast global abyssal plains [9,58,85,86]. It also cannot be denied that nodules and crusts are often found outside their typical precipitation depths. A distinctive pattern could be seen in the scavenging-type and the nutrient-type elements as to the metals associated with Mn or Fe (Figure 3) [58,79,87]. Mn and Fe show reversed distribution patterns throughout the ocean column, exhibiting a decreasing Mn/Fe ratio with deeper depths. Subsequently, the elements associated with Mn (Co, Ni, Te, Mo, W) and Fe (Cu, Ti, REY) also follow this trend and demonstrate similar patterns [7,58,67,68]. Mn-related elements generally show a lower concentration with deeper depths and Fe-related elements show higher concentrations. We exhibit in Figure 3 the critical metal contents to seawater depth based on the data of previous studies of global Fe-Mn crust and nodule contents versus their formation depths [67,85,88–92]. We also demonstrate, from previous correlation analysis, the relation between the metal contents of hydrogenetic Fe-Mn crusts and nodules and depth variations in the following decreasing coefficient order: Ti (0.77), La (0.58), Li (0.57), Cu (0.56), LREE (0.512), HREE (0.469), Y (0.354), V (0.272), Sb (0.25), Fe (0.229), Se (0.164), As (0.126), Zn (0.12), Cd (−0.02), Ce (−0.107), Tl (−0.154), Ni (−0.335), Mn (−0.345), Pt (−0.45), Te (−0.45), Co (−0.476), Mo (−0.69), W (−0.70), which reveals their distribution trends at deeper water depths [4,67,72,93]. In addition, seawater is also the main and direct source of the critical metals, many enriched critical metals in Fe-Mn nodules and crusts are derived from seawater at various water depths [25,68,87,94]. Other sources of the critical metals in seawater are mainly from terrestrial riverine input, groundwater input, hydrothermal input, aeolian input [4], weathering from underlying basaltic substrates [95] and cosmogenic inputs [96]. However, many elements show different and complicated

origins and sources, and the accurate distributions of the origins of many elements are still unclear.
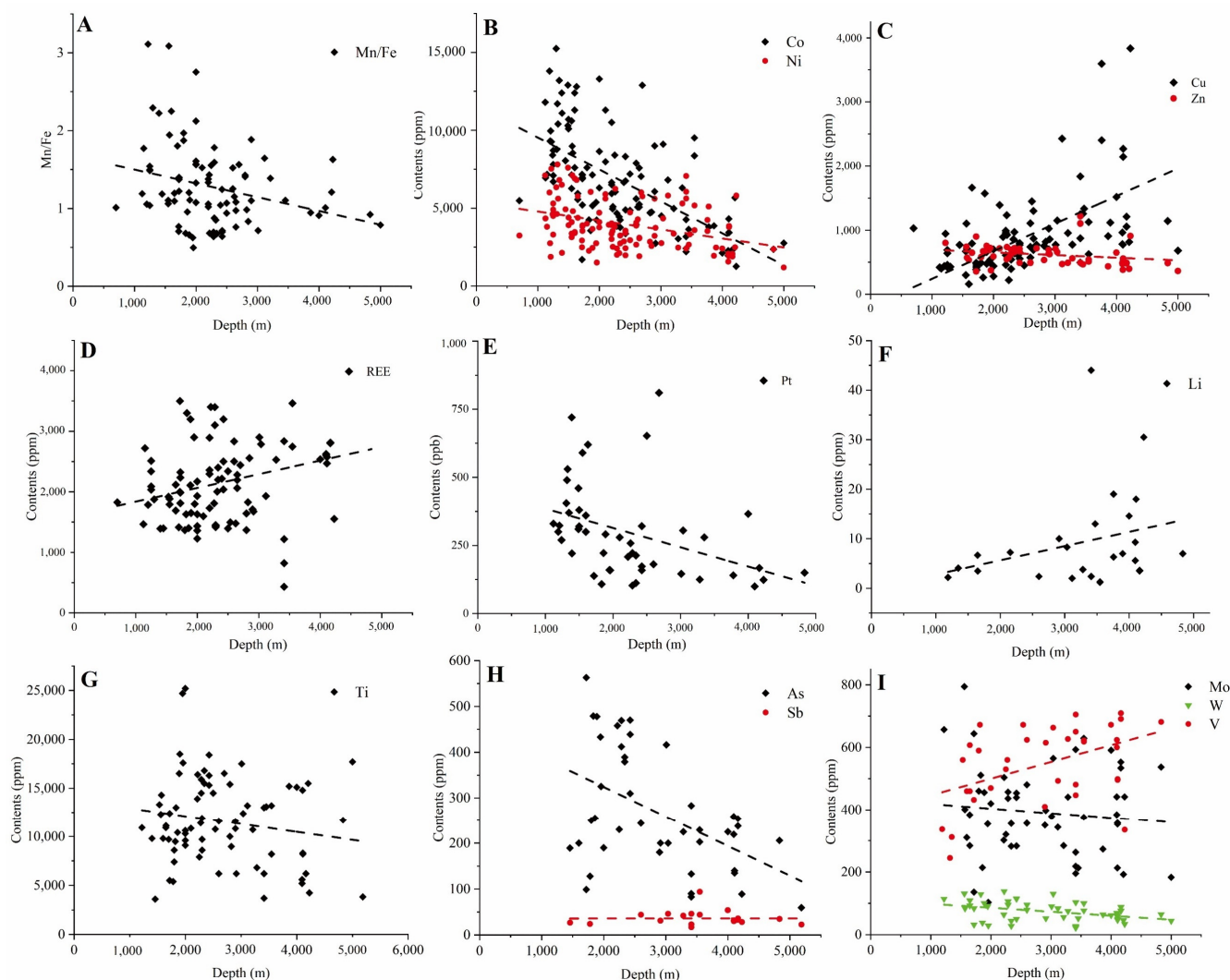

Figure 3. Critical metal abundance variations of hydrogenetic Fe-Mn crusts and nodules with seawater depths. The graph each shows the relation between water depth with (**A**) Mn/Fe, (**B**) Co and Ni, (**C**) Cu and Zn, (**D**) REE, (**E**) Pt, (**F**) Li, (**G**) Ti, (**H**) As and Sb, (**I**) Mo, W and V. Graphs and the trend lines are made and calculated from the data of [25,28,67,85,88–92].

3.4. Post-Depositional Phosphatization

Phosphatization occurs due to the increase in oceanic productivity in the upper water column and instigates compositional and mineralogical alterations to the younger un-phosphatized Fe-Mn crust layers. The older phosphatized Fe-Mn crust layers exhibit strongly altered textures and minerals by this epigenetic process [4,97–99]. Three major changes take place during this process (Figure 4): (1) the impregnations of carbonate–fluorapatite (CFA) and fine-grained phosphate materials. CFA is the characteristic mineral impregnated during this process. Alterations of elemental association and metal abundance that CFA causes are common and significant, e.g., REY and Cu undergo secondary enrichments [97,100–102]. (2) The reductive decompositions of Fe-Mn oxides in the new suboxic or anoxic environments. Porous Fe-Mn layers become subjugated by the suboxic waters of a vertically extended OMZ, and hydrogenetic oxides dissolve under this process and trigger metal releases, e.g., Co is significantly released [4,97,103]. (3) The recrystallization of tunneled diagenetic Mn mineral. The hydrogenetic Fe-Mn substance would be partially subjected to diagenetic remobilization, and vernadite will partially transform into tunneled

diagenetic Mn oxides, i.e., todorokite, causing diagenetic enrichment of certain elements, e.g., Cu and Ni [92,98,100,102]. However, the formation of the new diagenetic Mn oxides is generally in the early stages of their formation. Frequent occurrences of buserite and todorokite suggest that the hydrogenetic Mn precursors have been partly dissolved and recrystallized in the phosphatized crusts and undergone significant metal exchanges. REY, Pt, Cu and Ni which substitute for Mn are enriched in the phosphatized crusts due to the CFA occurrence and the diagenetic recrystallization [31,92]. The degree of disintegration and mineralogical recrystallization of the hydrous Fe-Mn oxide is controlled by the intensity of the phosphatization which decreases with deeper water depth [4,92,97]. Figure 5 shows the critical metal alterations under phosphatization based on the calculations of previous phosphatization studies. We find that REY, Li, Pt, Se, Cu and Te are generally enriched upon phosphatization, Co, Sb, As, Ti and W generally go through depletions upon phosphatization and Mo, V, Cd, Tl, Zn and Ni may show varied behaviors and show limited changes in contents during this period. We also suggest that Ni, Cu and Zn in the phosphatized layers are conflicted as previous reports suggested reversed results between enrichments and depletions [92,100–102]. Specifically speaking, their results found both high enrichments and high depletions for elements like Ni and Cu. We suggest that certain metal enrichments (e.g., Ni, Cu) during phosphatization are due to the metal remobilization to newly formed todorokite. However, the formation of todorokite may vary in different phosphatized samples, and todorokite formation in this period is also variable to compensate for the reductive dissolution of hydrogenetic MnO_2, i.e., the releases of Ni and Zn, therefore, occur in both enrichment and depletion.
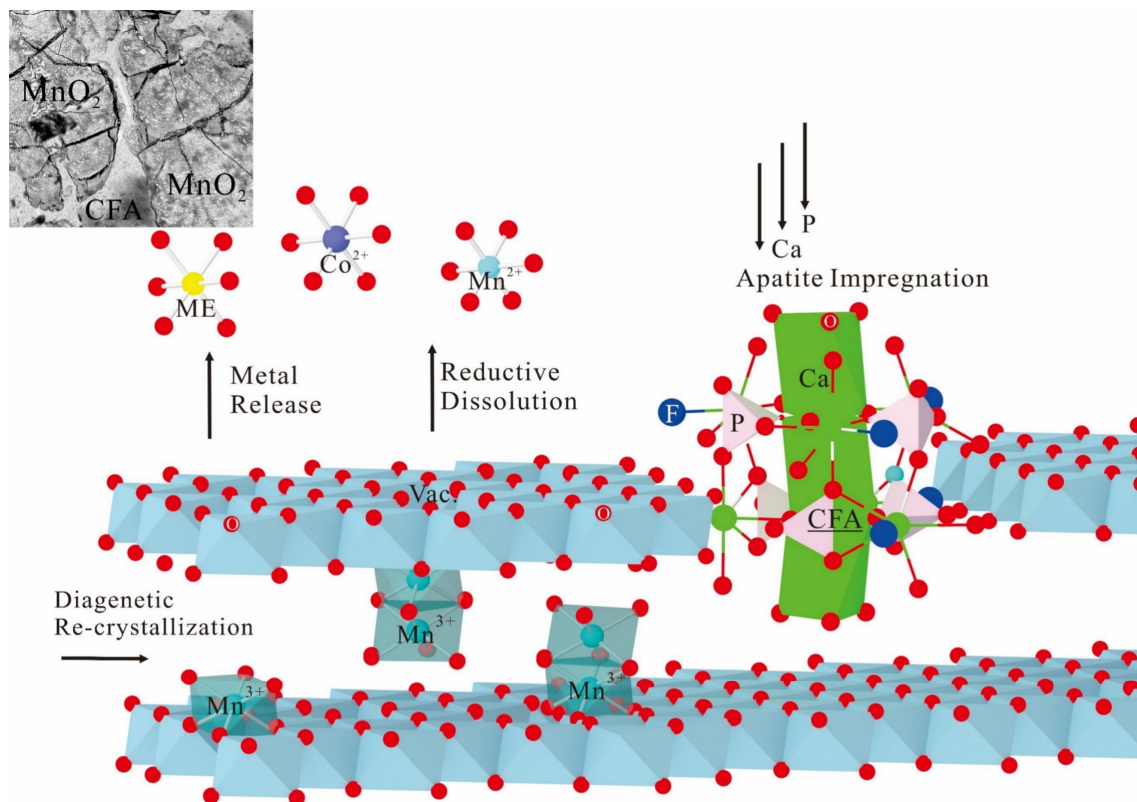

Figure 4. Schematic presentation of occurring processes in Fe-Mn crusts during phosphatization. Carbonate–fluorapatite (CFA) impregnation, lattice dissolution of Mn and critical metals, early diagenetic recrystallization. ME stands for metal. The red ball stands for oxygen. SEM image of CFA impregnation between hydrogenetic MnO_2 cavity corresponding to this model is inset in the top left.
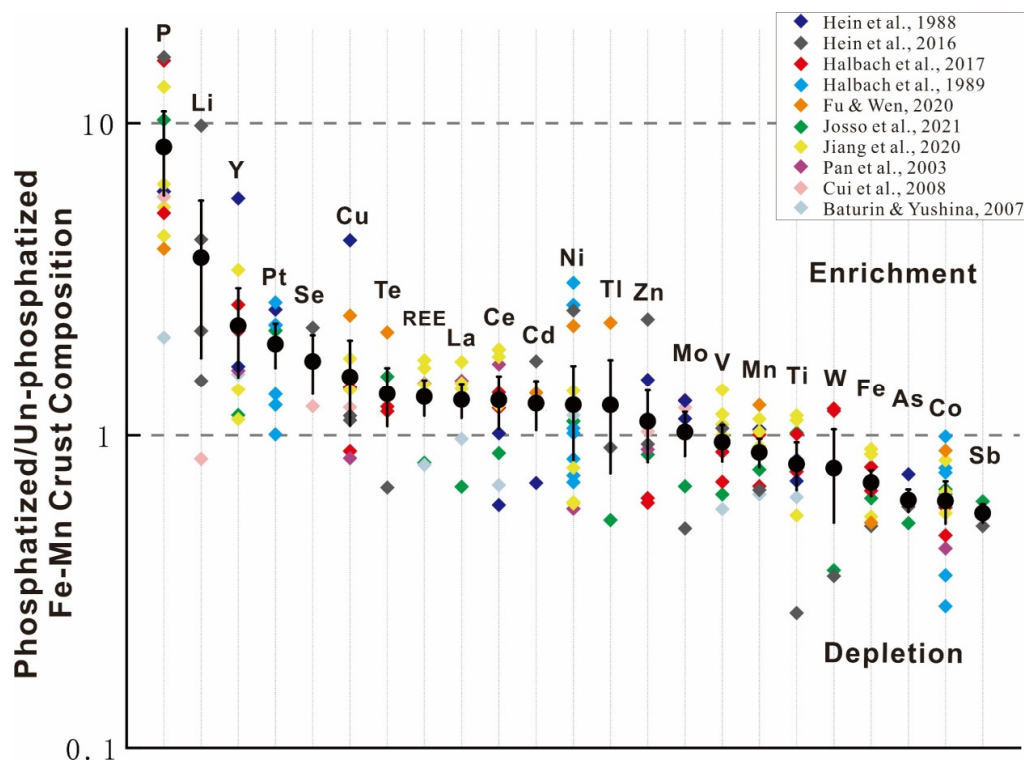
Figure 5. Alteration of the critical metals upon phosphatization. The black circle indicates average compositional changes, each diamond represents a phosphatized/un-phosphatized sample ratio, calculated from mean phosphatized Fe-Mn crusts normalized to the mean composition of un-phosphatized samples [4,72,85,90,92,93,99,101,102,104]. Varied colors represent applied data shown at the top right.

3.5. Structural Uptake

The high metal contents of marine Fe-Mn crusts and nodules are reflected by their micro-uptake mechanisms and mineralogical structures. Specifically speaking, the metal enrichments through a micro-perspective were commonly interpreted to explain how metals enrich into the layered or tunneled constituents of Fe-Mn crusts and nodules on an atomic scale [13,20,105,106]. Oceanic Fe-Mn crusts and nodules mainly consist of layered vernadite, buserite and 3-D tunneled todorokite, which are made up of octahedral MnO_6 nano-units and amorphous FeOOH that are intergrown with the Mn oxides [10,16,107–109]. The MnO_6 octahedrons comprise the Mn layer and the Mn tunnel structures, and they facilitate many isomorphic substitutions through Mn^{4+} or Mn^{3+} replacements and exhibit many vacant sites in the structures, i.e., unfilled empty octahedrons in the layer that attracts metal fillings [13,14,105,110,111]. The electro-charge deficits from low-valent cation replacements (e.g., $Co^{2+} \rightarrow Mn^{4+}$) can be balanced and compensated by the incorporations of hydrated cations in the interlayer or the tunnel center (e.g., Mg^{2+}, Ca^{2+}, Zn^{2+}, Li^+, Na^+). Interlayer cations and elements incorporated in the lattice also stabilize the Mn oxide's crystal structure [12,15,21,112]. For instance, reduction-produced Mn^{3+} during the crust phosphatization and the nodule burial often remain in the structure to help stabilize the Mn mineral and contribute to mineralogical transformation [14,113]. Thus, their mineralogical structures provide a high capacity for metal adsorption. The most common micro-uptake mechanisms for layered Mn oxides are the corner-sharing complexes that bond with two or three oxygens above or below the vacancy common in vernadite and birnessite (0.16 vacancy per Mn atom [114]), namely double corner-sharing (DCS) and triple corner-sharing (TCS). Incorporation (INC.) into the vacant sites often occurs from the corner-sharing sites [13,115]. The edge-sharing complexes in the parallel direction of the terminal edge site of the layer and direct/oxidative substitution of edge lattice Mn, namely

double edge-sharing (DES) and triple edge-sharing (TES) [115–118]. Tunneled Mn oxides in nodules and crusts showed common sorption approaches in tunnel-center and tunnel-wall occupation. Large-radius cations such as Mg, Ca, Li and Tl and critical metals such as Ni and Cu tend to sorb onto the tunnel center and tunnel wall [14,36,105,119]. The critical metals are attracted to the Mn oxides to exchange with surface $Mn^{3+/4+}$ and form metal (ME)-O bonds or -OH bonds in the octahedral layers or tunnels. Foremost are the corner-sharing and edge-sharing coordination modes in marine vernadite with ample vacancies [120–122]. High ME/Mn ratios could lead to rapid vacancy depletion or blockade and, under this scenario, the edge-site coordination, which is the least constrained position, grows to be increasingly common as the layer becomes filled [116,123,124]. The high critical metal uptake is not irreversible, especially under reductive dissolution when the seawater redox condition changes via microbial/abiotic reduction, covered by anoxic seafloor sediments or a reducing phosphatization event occurs. The reduction of Mn^{4+} to $Mn^{2+/3+}$ and more seawater $Mn^{2+/3+}$ compete for viable sorption sites. Metal-filling lattice dissolution also inevitably inhibits adsorption capacity. The extensive simulations of metal adsorption on $Mn^{2+/3+}$-rich δ-MnO_2 have explained that the decrease in the Mn oxidation state and reducing systems are detrimental to critical metal adsorption [62,120,125]. Specifically, the prominent sorption positions (corner sharing and incorporation in the layer) are competed by low-valent Mn, causing other metals to sorb to the edge-sharing sites at layer rims [62,122,125].

4. Categorization of Critical Metal Enrichment Pathways and Coordination

In our study of critical elements enriched in marine Fe-Mn crusts and nodules, we conclude five major enrichment pathways for critical metals enriched in Fe-Mn (oxy)hydroxides based on the major host phases, the occurrence of oxidative enrichment and the prevalence of chemical exchange and structural incorporation with respect to previous experimental evidence:

(1) Direct substitution for Ni, Cu, Zn and Li through surface complexation predominantly on the δ-MnO_2 surface [21,38,110,117,124,126]. For these univalent elements, direct surface complexation is most prominent during the adsorption onto marine Fe-Mn oxides. Ni, Cu, Zn and Li have shown large inner-sphere complexes on mineral surfaces (Li also showed outer-sphere sorption in carbonate phase and tunnel-wall site), while Mn oxides generally show a much larger contribution to elements of this group [32,33].

(2) Oxidative adsorption for Co, Ce and Tl which mainly enrich through an oxidation–substitution mechanism with δ-MnO_2 [15,20,62,69,118,127,128]. Redox-sensitive elements in seawater remain at a lower valence and are oxidized by MnO_2 through substitution in oxic environments. Co, Ce and Tl are preferentially oxidized to the less-soluble inner-sphere higher-valence species in the Mn oxides, while insoluble oxidized species participate less in the exchange reactions and are progressively accumulated over a prolonged duration and eventually exhibit an extraordinary abundance, thus obtaining a high correlation to Mn.

(3) Partitions between δ-MnO_2 and amorphous FeOOH for REY, Cd, Mo, W and V [24,33,63,129–133]. REY (except for Ce) possess both negative and positive species in seawater, generally showing complex preferences of LREE-CO_3^+ and HREE-CO_3^{2-} and exhibiting sorption preferences to both the Mn oxides and Fe oxyhydroxides, causing a partitioned distribution between Mn and Fe phases. Cd with both negative and positive chloro-species also fits this description. Mo, W and V accumulate through inner-sphere surface complexation, although all being anions in seawater, an electro-repulsion breakthrough to partially sorb with δ-MnO_2 has been observed, causing partition by both phases.

(4) Combined enrichments of Mn-phase oxidative uptakes and Fe-phase structural incorporations and adsorptions for Te, Pt, As and Sb [26,31,34,61,64,134–143]. For these multi-valent critical metals that reside as seawater anionic species, in addition to the natural electro-driven adsorption onto FeOOH, their low-valent species Te^{4+}, Pt^{2+}, As^{3+} and Sb^{3+} are observed with common oxidative enrichments on δ-MnO_2, whereas high-valent species, Te^{6+}, As^{5+} and Sb^{5+}, are likely structurally incorporated by Fe oxyhydroxides without the occurrence of oxidation. Different from simple partitions like Cd or REY, this pathway

shows dual contributions of Mn-oxidative enrichments and Fe incorporations which vary in their mechanisms.

(5) Dominant uptake by amorphous FeOOH for Ti and Se [25,32,144,145]. These elements are mostly sorbed onto Fe oxyhydroxide and enriched in its structure. They are considered highly Fe-associated elements, Ti in particular.

We also categorize the major coordination preferences in layered vernadite and tunneled todorokite structures in Figures 6 and 7. We conclude that in layer-type birnessite or vernadite, Co, Ni, Cu, Zn and Tl commonly occupy as TCS complex above or below the vacant sites [13,20,116,123]. Co, Ni and Cu could also partially or completely enter the layer vacancies to be layer incorporated (Co is mostly incorporated, Ni may cause layer distortion when incorporated in the layers and Cu is less observed in INC.), whereas Pt becomes incorporated through substitution with Mn in the layer [31,61]. As, Sb, Mo, W, V and Te commonly occupy DCS complexes in the Mn layers [26,37,63,134]. Less competitive DES sorption sites at the terminal edges of the Mn layer are common for Ni, Cu, Tl, As, Sb, W and Mo [106,122,124], especially when a lack of layer vacancy occurs, as this sorption site is metal attractive and less restrained for metal to sorb onto. DES modes are also common for corner-sharing metals when they are less competitive to take up corner-sharing positions or are forced out of corner-sharing positions. REY are all inner-sphere surface complexed, but their detailed coordination mechanism requires further investigation [24,46]. In tunneled todorokite, prominent sorption positions are loosely bound hydrated tunnel center and surface complexation in or on the tunnel wall. The enrichments of many critical metals in todorokite and their specific sorbed positions are scantily understood due to the complexity of the structure. Some seawater-derived metals, e.g., Co, REY and Te, are less enriched in suboxic todorokite, leading to difficulties in their investigations. Elements rich in marine sediment and prone to diagenetic enrichment (e.g., Ni, Cu and Li) show high abundances and clearer understandings [14,36]. Divalent cations like Ni, Cu, Zn and Cd are observed to occupy both the tunnel-wall and hydrated center-tunnel positions, while Tl^+ and Li^+ are insufficient to compensate the surface electro-deficits, showing preferences to occupy the hydrated tunnel center [36,105,119,146,147].
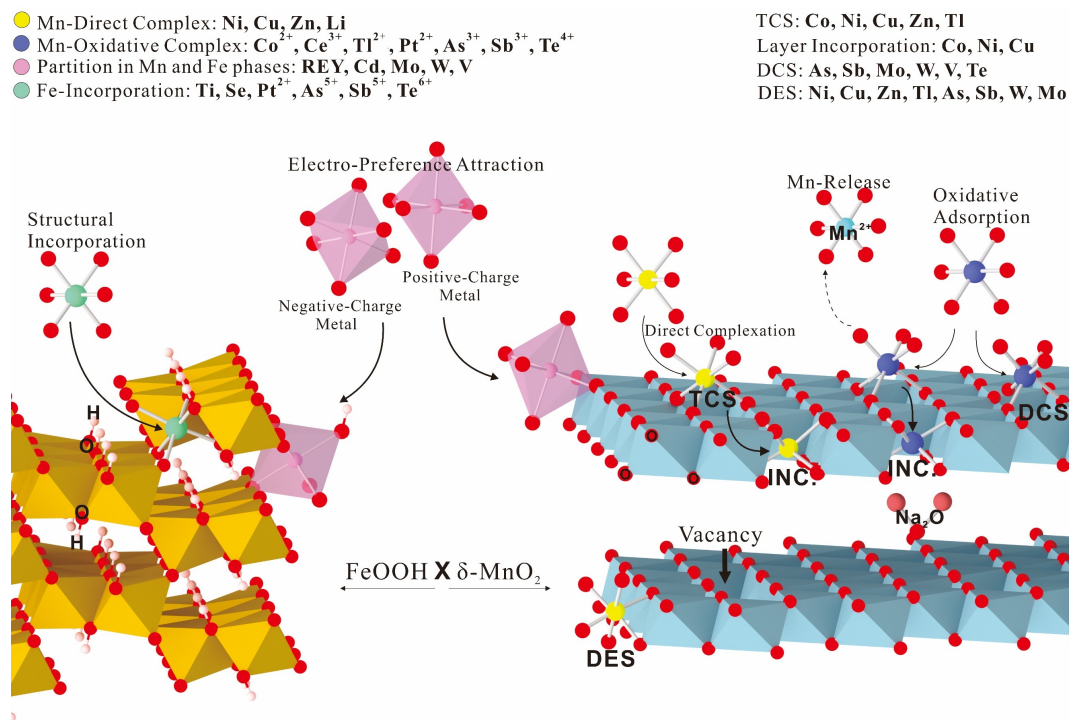

Figure 6. Schematic presentation of major enrichment pathways in hydrogenetic Fe-Mn (oxy)hydroxides. Major enrichment pathways and associated enriched metals correspond to color

legend in the top left. Major metal configurations and associated metals are marked in the top right. TCS: triple corner-sharing position above layer vacancy, DCS: double corner-sharing position, DES: double edge-sharing at the layer terminal, INC.: metal incorporation into the layer from interlayer.
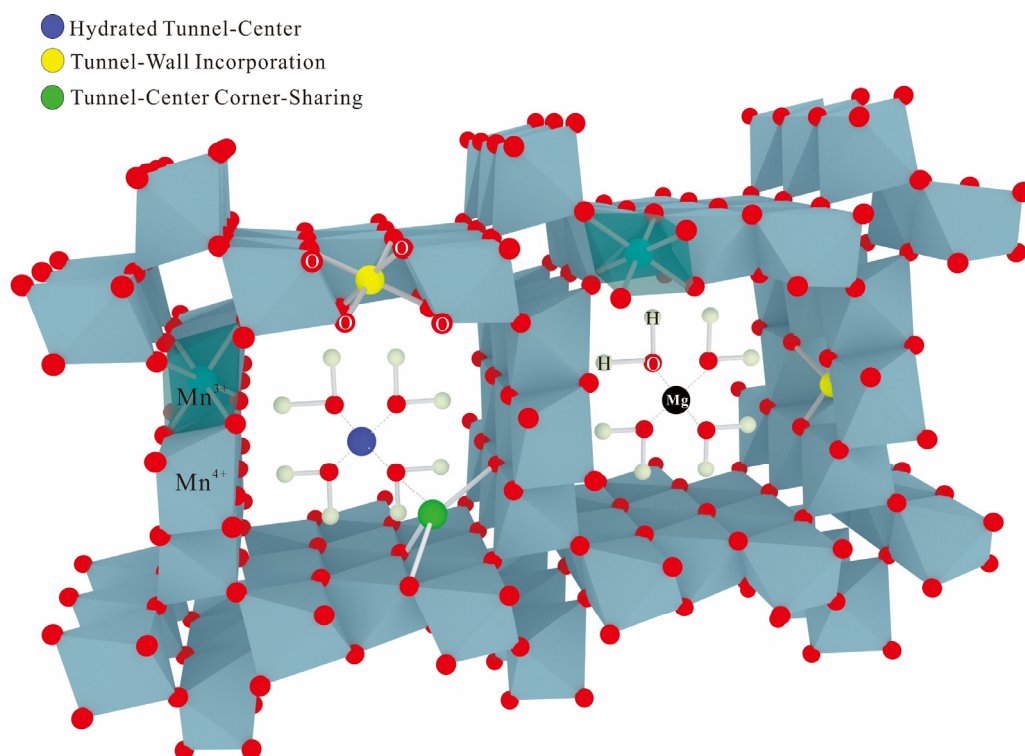

Figure 7. Schematic presentation of major metal coordination in diagenetic tunneled todorokite. Large-radius cations like Tl, Li, Cd, Mg, Ca and Na are prone to occupy tunnel center, Ni, Cu, Zn can occupy central position but also tend to occupy edge-sharing and corner-sharing positions in the tunnel and wall incorporation [36,105,119,147]. Colored configurations correspond to top-left legend.

It is necessary to note that many of these observations were conducted on synthetic Fe-Mn (oxy)hydroxide samples, e.g., synthesized birnessite, todorokite, ferrihydrite and goethite, rather than on the natural poorly crystallized marine vernadite and amorphous FeOOH, which may show distinct variations in metal enrichment pathways and coordination preferences. Previous experimentations have also prioritized simulating metal behaviors in the hydrogenetic conditions rather than the suboxic–diagenetic environments. Further research aimed at the critical metal enrichment mechanisms and coordination preferences still requires many experiments to explain unsolved problems in the critical metal enrichments in natural Fe-Mn crusts and nodules, and our categorization only provides an understanding of current experimental knowledge.

5. Elaboration of Critical Metal Enrichment Characteristics and Mechanisms

5.1. Major Ore-Forming Metals: Cobalt, Nickel, Copper and Zinc

5.1.1. Cobalt and Nickel

Co and Ni are the most characteristic ore-forming critical elements enriched in marine ferromanganese crusts and nodules [51,68]. The depositional environment and genesis highly influence Co contents. High Co enrichment occurs in oxic hydrogenetic conditions, with mean Co contents varying between 6662 ppm in hydrogenetic crusts of the PPCZ to 475 ppm in diagenetic nodules of the Peru Basin [2,5,148], Co contents with pure hydrogenetic influence may reach up to 1–2% [4,11]. Co demonstrates a high positive correlation with Mn and a dominant Mn host phase in hydrogenetic oxides [32,33,59,68]. The negative

correlation between Co and Fe weakens with increasing depths and disappears in deeper waters and the marine sediment [43]. In hydrogenetic Fe-Mn crusts, Co has been explained with a prevalent oxidative substitution mechanism, in which dissolved Co^{2+} in seawater will be progressively oxidized to insoluble Co^{3+} by the near $Mn^{3+/4+}$ on the δ-MnO_2 surface [15,20,68,149]. The insolubility greatly inhibits further surface–seawater reaction, which also promotes progressive accumulations. Takahashi et al. [20] revealed that Co in crusts and nodules was all trivalent, while only a small fraction of sorbed Co was observed as divalent on the Fe phase, which indicates its exclusive redox mechanism. The high Co uptake is also radius feasible, as the atomic radius of Co^{3+} (0.54-Å) is close and similar to the layer-composing Mn^{4+} (0.53-Å) [20]. Co is gradually incorporated into the layer upon oxidation by the nearest Mn or by the direct replacement of TCS Mn^{3+}. Repetitions of these processes lead to high Co enrichments [15,149]. The majority of Co is structurally incorporated into the Mn layer after TCS sorption, and Co can also sorb in edge-sharing sites which is analogous to layer incorporation [13,62,120]. The pH condition is crucial in the transition from TCS to structural incorporation and, at alkaline seawater pH, the majority of Co adsorbed will be eventually incorporated into the Mn layers [13,15,150,151]. Co enriched in oxic seawater likely undergoes evident dissolution under phosphatization, and hydrogenetic MnO_2 dissolves or transforms under phosphatization, with either process releasing Co. Co sequestration loss has been reported at around 30% to 50%, hence having a significant impact on the Co enrichments [14,92,100,102]. Low Co enrichments through diagenetic uptakes were also investigated, and a positive Co-Fe association was observed in diagenetic nodules, indicating the sorption by Fe phase in diagenetic nodules [6,12]. It was argued that Co under diagenetic conditions was ineffective in replacing $Mn^{3+/4+}$ because of incompatible crystal field stabilization energy and ionic radius, and Fe hydroxides in this environment became more adsorbent for Co [7,84]. However, sequential extraction of diagenetic samples still revealed Mn as the main host phase [59]. Many in situ analyses have also indicated that, in diagenetic nodules, Co-rich areas are still evidently vernadite or buserite formed in oxic pore-water space rather than todorokite [12,107,152], showing that Co prefers to sorb onto hydrogenetic Mn oxides even in diagenetic conditions.

Single-valent Ni^{2+} shares similarities with Co in the dominant correlation and the host phase with Mn in hydrogenetic growth, but it also shows higher contents in diagenetic nodules. Ni varies between 2581 to 4643 ppm under hydrogenetic conditions and is significantly enriched with diagenetic inputs. Nodules from CCZ have shown an average Ni content of 1.3% [21,32,150]. Previous elemental mapping, correlation analysis and sequential leaching results all disclosed high Ni affinity with the Mn oxides in hydrogenetic and diagenetic conditions, exhibiting positive Ni-Mn relations in enrichment [10,21,33,59]. Structural substitution and interlayer sorption in layered and tunneled MnO_2 make up the main Ni enrichment mechanism in both diagenetic and hydrogenetic crusts and nodules [119,121,152,153]. Inner-sphere surface complexations through TCS and the gradual layer incorporations into the vacancy, which suggest a cation-exchange mechanism in which Ni replaces Mn through isomorphic substitution, are dominant for Ni enrichment [116,121,153,154]. The Ni-TCS adsorption, which acts as a transitional mechanism, has been suggested as a necessary waystation towards the structural layer incorporation as the direct incorporation into the layer from seawater was not observed [116,153]. Alkaline pH conditions lead to an increased proportion of Ni incorporation [110,153,155]. Therefore, a moderate seawater pH environment and sufficient sorption time in hydrogenetic Fe-Mn crusts and nodules are critical for Ni and other critical metals' sorption and eventual layer incorporation [121,150]. However, the Ni loading (also for other metals) in the Mn mineral is not affected by pH, and pH only regulates metal coordination. This is in sharp contrast to findings that suggest high pH increases Ni enrichments [121,155]. Ni contents are more significant under diagenetic conditions [6,36,67]. Ni contents in diagenetic nodules show a positive relation with increasing Mn/Fe [12], and the high Ni contents in diagenetic Mn oxides could be derived from Ni cycling in the seafloor sediment and the suboxic pore-water space [6]. Simulations by Kim and Kwon [105] suggested that Ni could be pref-

erentially adsorbed in the tunnel of hydrated todorokite. The Ni behavior upon diagenetic transformation also shows significant impacts on the Ni enrichments. Metal sequestration is released up to 50% during the dissolution of layered Mn oxides, followed by the readsorption of the released Ni into the new tunnel oxide (Figure 5) [111,119]. The effects of phosphatization on Ni are the subject of conflicting reports in both enrichment [90,97,102] and depletion [67,92,101]. Ni upon phosphatization is remobilized to newly formed stable todorokite after prior release from the layered hydrogenetic MnO_2 and becomes further enriched. Thus, we suggest that Ni in the phosphatized crusts resides mainly in newly transformed todorokite, but todorokite formation may vary in different samples, regions and other dynamic conditions and, hence, vary in Ni enrichment or depletion.

5.1.2. Copper and Zinc

Cu and Zn are important ore-forming critical metals in Fe-Mn crust and nodule formation and are suggested to stabilize the structure of Fe-Mn (oxy)hydroxides and compensate for the surface electro-charge deficits [13]. Cu and Zn are better enriched under diagenetic conditions than under hydrogenetic conditions. Cu in the CCZ and the Peru Basin with high diagenetic inputs exhibited a mean value of 10,600 ppm and 5988 ppm, whereas Cu in hydrogenetic crusts from the PPCZ only showed 976 ppm. Simultaneously, Zn in the CCZ and the Peru Basin showed values of 1385 and 1845 ppm and in the PPCZ hydrogenetic crusts showed 668 ppm [2]. Thus, they are more likely incorporated in the diagenetic 10-Å manganates [12,22,36]. It is noteworthy that the Peru Basin, as a representative diagenetic nodule region, showed much lower Cu contents compared to the CCZ [5]. Wegorzewski and Kuhn [6] have attributed this discrepancy to the different chemical compositions of the local CCZ siliceous and the Peru Basin calcareous marine sediments. Cu as a nutrient-type element shows a larger sorption efficiency in the suboxic oceanic sediments than the hydrogenetic scavenging from overlying water [36,87,117]. Previous examination of Cu distribution in the oceanic sediments and the growth structures within the nodules found only insignificant Cu in the upper 20 cm of nodule-rich sediments, where Cu was dominantly associated with the diagenetic growth within the nodule, indicating effective scavenging by diagenetic 10-Å manganates [36,84]. As important lattice-filling and deficit-compensating elements in diagenetic todorokite, Cu and Zn occupy both the hydrated tunnel center or form corner-sharing complexes within the Mn tunnel wall [36,105,147]. The enrichments of Cu and Zn in hydrogenetic conditions were also highly studied. Cu and Zn in hydrogenetic crusts and nodules have been suggested to be associated with Mn phase, and in situ mapping and correlation analysis showed Cu and Zn distributions in crusts and nodules were mainly correlated with Mn-rich areas, instead of Fe phase [12,117,156]. However, sequential leaching and sorption experiments also suggested that Cu and Zn in hydrogenetic crusts could be also partially, or even highly, adsorbed in Fe phase, which requires subsequent investigation [31,33,59,157]. The adsorption mechanisms of Cu and Zn in hydrogenetic layered MnO_2 occur through direct substitution and occupation of the available vacant sites. Specifically, Cu and Zn sorb through TCS configurations in the δ-MnO_2 at the expense of vacant sites and $Mn^{3+/4+}$. Partial Cu and Zn are also adsorbed in the hydrated interlayers as electro-compensating cations [117,156,158,159]. Various experimentations have found that a proportion of Cu in hydrogenetic MnO_2 could be inner-sphere incorporated into the Mn layer from the TCS position [117,124]. However, Zn was observed to be exclusively enriched in the TCS configuration above layer vacancy, that Zn was not likely incorporated in the Mn layer [13,156,159]. The fact that Zn was mostly observed as an undistorted octahedral species in the Mn layers in oxic seawater also concurs with this finding [126,160]. In addition to TCS enrichments, alternative DES configurations would be more dominant in high metal loadings or in less oxidized environments for Cu and Zn enrichments. Less competitive Cu and Zn may preferentially enrich onto Mn-layer edges than the Mn layer [62,122,124,126]. Additionally, Cu and Zn both show evident increases in contents upon phosphatization events (Figure 5) [92,97,102]. Diagenetic 10-Å manganates and CFA formed during this stage are likely to enhance Cu

and Zn enrichments because Cu and Zn are more prominently enriched in Mn phase and the residue phase after phosphatization alterations [33,97].

5.2. Rare Earth Elements and Yttrium (REY)

REY concentrations vary between 2454 ppm in hydrogenetic crusts from the PPCZ to 403 ppm in diagenetic nodules from the Peru Basin. Hydrogenetic conditions uniformly show higher REY contents and have been extensively studied [25,42,161–163]. As scavenging-type elements, REY sequestered in Fe-Mn colloidal particles largely originate from seawater and only a small fraction of the REY contribution is from the oceanic sediments. Hydrogenetic δ-MnO_2 and hydrated $FeOOH$ are considered effective REY adsorbents, as their large spaces in structures potentially accommodate great amounts of REY [46,76,87,161,164]. But diagenetic 10-Å manganates, which exhibit inferior abilities to incorporate REY, are less discussed. The enrichment mechanism of REY(III) from seawater primarily occurs through surface complexations on the Fe-Mn (oxy)hydroxides [25,46,89,165,166]. REY in seawater are 89% carbonate complexed with a minor fraction being free REY cations [60]. Generally, they exist as LREE-CO_3^+ and HREE-CO_3^{2-}, which direct their sorption preferences onto δ-MnO_2 and amorphous $FeOOH$. Upon REY adsorption on the surface of the Fe-Mn oxides, the ligand exchanges between the carbonate and the hydroxyl are induced [129,161,164,167]. Hydrogenetic REY distribution generally shows an increasing proportion in Fe phase and a decreasing proportion in Mn phase from La to Yb, which suggests that Mn phase and Fe phase show preferences to REE adsorptions, each relatively adsorbing more LREE and HREE [24,46,91,165,167]. It is noteworthy that in some unique cases, the residue phase may also contribute to REE enrichments up to 30% in Fe-Mn crusts, e.g., Detroit Guyot that is under strong terrestrial material inputs [168]. Alkaline seawater pH and slow growth rates also yield higher REY concentrations and allow for efficient REY removal from seawater [24,47,77,169]. Reports on Fe-Mn crusts from the South China Sea with an elevated growth rate contributed by terrigenous materials demonstrate a lower REY abundance in comparison to the West Pacific typical hydrogenetic Fe-Mn crusts [24,46,74,77,129]. Phosphatization also elevates REY abundances to a great extent. REY concentrations are significantly enhanced from 20% to 50% during phosphatization events [4,25,92,102], and a possible REY enrichment mechanism through large-radius cation (Ca, Na and Si) replacement during CFA impregnation was also proposed [92].

Ce and Y are two elements with high emphases among REY and have been often discussed individually for their redox condition's determination and application in genesis discrimination in oceanic Fe-Mn crusts and nodules [24,77,169,170]. Ce enrichments through surface complexation and oxidative scavenging by Fe-Mn (oxy)hydroxides were widely examined [69,166,169,171]. Seawater Ce^{3+} has been revealed predominately as Ce^{4+} in hydrogenetic crusts and nodules after surface reactions [20,69]. Ce oxidative enrichments on δ-MnO_2 were widely detected and a high positive Ce-Mn association was exhibited. Similar to Co, soluble Ce^{3+} was oxidized by Mn^{4+} to insoluble Ce^{4+} by Mn substitutions [20,24,25,69]. However, Ce enrichment contributed by Fe phase has yet to be aligned. De Carlo and Wen [169] have exhibited that proportional Ce could be adsorbed onto Fe oxyhydroxides through surface complexations in a similar manner to other REY^{3+}. Bau [163,166] argued with evidence of Ce oxidative enrichments on Fe oxyhydroxides. We find that Ce distributions in different samples and results also show large variations between Mn and Fe phases [20,166], i.e., studies showed that both Mn and Fe phases could be dominant Ce adsorbents. In any case, the evident Ce oxidative scavenging and high Ce abundance make Ce unique among REY enriched in oceanic Fe-Mn deposits [24,69,166,169]. Y, on the other hand, shows similar behavior to other HREE-CO_3^{2-}. Negatively charged Y is preferably partitioned by Fe oxyhydroxides through surface complexation, corroborated by a positive Y-Fe association and the dominant Y enrichment contribution from Fe phase [2,25,166]. Y exhibits a higher concentration of 61–132 ppm in hydrogenetic Fe-Mn (oxy)hydroxides [46,77,172] and commonly shows high alteration due to post-depositional

phosphatization events. Y contents are noticeably enriched as a result of phosphatization (Figure 5).

5.3. Platinum Group Elements

Platinum group elements (PGEs) consist of Ru, Rh, Pd, Os, Ir and Pt. PGE abundances in seawater are exceptionally low: Ir: 0.0013 ppb; Ru: 0.002 ppb; Rh: 0.09 ppb; Pt: 0.19 to 1 ppb; and Pd: 0.04 ppb [95,173,174]. But PGEs are significantly enriched in marine ferromanganese crusts and nodules. In particular, Pt is enriched up to more than 100 times compared to the Earth's crust and the seawater value [42,175]. Pt is the most highly enriched PGE with a mean abundance of 408 ppb for crusts and 181 ppb for nodules. Extreme cases of Pt enrichment may reach up to 1–3 ppm in hydrogenetic crusts [93,175], and other PGEs are also enriched evidently in Fe-Mn crusts (Ru, Rh, Pd, Os, Ir are respectively enriched to 16 ppb, 16 ppb, <7.3 ppb, 2.5 ppb, 5.1 ppb) [31]. Previous studies have sufficiently determined the association of PGEs with water depths, growth rates and regional characterizations. The negative PGE correlations with the growth rates and the water depths were examined as influencing factors to form higher PGE enrichments [176–181].

Platinum is the most highly investigated and the most enriched PGE in Fe-Mn crusts and nodules [31,93,175,178]. Pt has been described to be negatively correlated to water depths and the growth rates of the Fe-Mn adsorbents, as slow-growing Fe-Mn crusts in shallower depths contain relatively higher Pt [4,93]. Pt species in seawater have been determined to exist mainly as divalent chloro-complexed $PtCl_4^{2-}$ or hydrolyzed $PtCl_3OH^{2-}$ and tetravalent chloro-anion $PtCl_6^{2-}$ or hydrolyzed $PtCl_5OH^{2-}$ [60,93,174,182]. A unique Pt enrichment pathway explains that Pt^{2+} can be both oxidatively enriched to Pt^{4+} in hydrogenetic δ-MnO_2 and adsorbed in feroxyhyte despite remaining as a negative species [4,31,61]. Seawater Pt complexes are negatively charged, and all seawater Pt should be adsorbed onto the Fe oxyhydroxides. However, sequential leaching and correlation analysis have revealed the occurrences of evident Pt oxidative enrichments by Mn phase and positive Pt-Mn association [31,67]. XAS observation has also found that Pt^{2+} was adsorbed on δ-MnO_2 through oxidative enrichment [31,61]. Koschinsky et al. [31] suggested that the electrostatic repulsion between the Pt complex and the Mn oxide was overcome and that a preferential Pt^{2+} binding onto Mn phase became possible. Thus, Pt^{2+} is enriched and oxidized to Pt^{4+} in hydrogenetic MnO_2 through oxidative substitution and forms Mn-O-Pt bonds [31,61]. The positive relations between Pt and other redox-sensitive elements (Co, Ce and Tl) were shown, which reflect similar behavior driven by oxidative interaction [4,31,95,178]. As for electro-chemically favored Fe phase, simple electro-driven adsorption and co-precipitation were suggested for Pt enrichments as no oxidation of Pt was observed on Fe phase [31]. δ-FeOOH (feroxyhyte) mainly enrich Pt^{2+} and partial seawater Pt^{4+} as indicated by XANES results [31,61]. However, a recent study has shown Pt might be oxidatively enriched on goethite by dissolved O_2 through the dehydration–condensation process, while FeOOH acts as an oxidative catalyst [183]. What is also worth mentioning is that all Pt in natural Fe-Mn samples was observed to exist predominantly as high-valence Pt^{4+} [31], suggesting that Pt enrichment in natural samples varies with experimental results regarding Pt^{2+} enrichment. PGEs are highly enriched by phosphatization events, and an increase in PGE contents in the phosphatized crust was widely observed (Figure 5) [4,31,93]. Higher Pt contents in the phosphatized layers are caused by the post-depositional diagenetic processes. Previous correlation analysis does not support a positive Pt-P relation, which implies that Pt is not incorporated or enriched in secondarily formed CFA, but stable diagenetic todorokite formed under this process [4,31]. The inhibitory effects of phosphate material on Pt enrichment by Fe phase also suggest that seawater Pt enriched in Fe oxyhydroxides may undergo host-phase transfer to Mn phase during phosphatization events [183].

5.4. Dispersed Elements

Among the eight dispersed elements, Te, Tl, Se and Cd are enriched in the marine ferromanganese crusts and nodules compared with the Earth's crust and pelagic clay [72].

Under hydrogenetic and hydrogenetic–diagenetic (mixed) growth, Cd, Se, Te and Tl are enriched in marine Fe-Mn deposits mainly by adsorption onto the δ-MnO$_2$ and amorphous FeOOH [72]. Among the four enriched dispersed elements, only Cd does not have multi-valence properties, and the oxidation occurrences during the enrichment processes are prevalent for Te, Se and Tl, which are redox sensitive in Fe-Mn crusts and nodules [34,127,145,184]. Fu and Wen [72] have conducted a comprehensive analysis on Cd, Se, Te and Tl and revealed data-based variation patterns in their relations with the water depths and sample depths. This segment elaborates on the enrichment characteristics and processes of Te, Tl, Se and Cd in marine Fe-Mn crusts and nodules.

5.4.1. Tellurium

Tellurium has a low abundance of 1 ppb in the Earth's crust, but Te is the most enriched element in hydrogenetic Fe-Mn crusts. Te has an enrichment factor of up to 50,000 times (Figure 1) with a mean value of 46 ppm in hydrogenetic crusts. Te is a highly hydrogenetic metal originating from seawater, and the highest Te contents are observed in hydrogenetic crusts, whereas Te only displayed insignificant enrichment in diagenetic nodules [26,72]. However, studies regarding Te enrichments in oceanic Fe-Mn crusts and nodules are rather few, considering its high enrichment. The Te speciation in seawater has been proposed as HTeO^{3-}, H$_5$TeO^{6-} or TeO(OH)$^{3-}$ and TeO(OH)$^{5-}$ [60,185,186]. Te in seawater as a tetravalent or hexavalent hydrated oxyanion would be attracted to positively charged amorphous FeOOH, which is in good agreement with previous sequential leaching that showed more than 80% of Te in hydrogenetic crusts and nodules was enriched on Fe oxyhydroxides, while partial Te enrichments were contributed by Mn phase [33,187–189]. Hein et al. [26] proposed that the high Te enrichments can be caused by the oxidation from Te^{4+} to Te^{6+} on the FeOOH surface. However, Kashiwabara et al. [34] conducted co-ordination observation and found that no Te oxidation process occurred in ferrihydrite, instead, oxidations of Te^{4+} to Te^{6+} were detected upon enrichment onto hydrogenetic layered MnO$_2$. Thus, Te^{4+} was suggested to be only oxidatively enriched on δ-MnO$_2$, whereas on the ferrihydrite surface, Te^{4+} was enriched through electrostatic adsorption and Te^{6+} can be predominately incorporated through co-precipitation due to similar molecular geometry to Fe^{3+} octahedrons [34]. It is noteworthy that Te in natural Fe-Mn crusts has been suggested to be solely Te^{6+} [34], therefore, we suggest that Te in hydrogenetic Fe-Mn crusts and nodules is mainly enriched through a unique combined enrichment pathway between Fe structural incorporation and Mn oxidative enrichment. Phosphatization generally enriches Te, and the older crust layers from Magellan Seamount (76.5 ppm) exhibited twice the value of the younger layer (33.8 ppm) [4,102]. The detailed mechanism of Te enrichment during phosphatization is not yet known, but host-phase transfer and enrichment of Te from Fe phase to newly formed stable Mn phase may be responsible as previous studies showed phosphatization hinders Fe incorporation and induces reductive dissolution [97,183]. Tellurium, as the most enriched element in marine Fe-Mn deposits, is shrouded with many unknowns (e.g., the low contribution from MnO$_2$ indicated by leaching and XAFS data cannot explain the high correlation between Te and Mn), and the current explanation requires more investigation and progress to explain its high enrichment [26,72].

5.4.2. Thallium

The average Tl contents of major oceans range from 41 to 160 ppm in Fe-Mn crusts and from 129 to 347 ppm in Fe-Mn nodules [2], and Tl shows a high enrichment factor of more than 100 times compared to the Earth's crust (Figure 1). Tl exhibits negative relations with the Fe-Mn mineral's growth rates and water depths and endures significant enrichment upon phosphatization [4,102]. The majority of dissolved seawater Tl generally exists as Tl$^+$, and to a lesser extent, as TlCl and Tl(OH)$_4^-$ [60]. Similar to many other redox-sensitive elements, under hydrogenetic conditions, Tl is favored in oxidative enrichment through Mn substitution [118,123,127,190]. The availability of Tl oxidative enrichment has been suggested to be partly determined by the mineralogical composition of the Fe-Mn adsorbent,

specifically, the reactivity and capacity of sorption sites in the layered structure [62,115,190]. The oxidation of Tl^+ to Tl^{3+} almost exclusively occurs in hexagonal birnessite, which is characteristic for having vacancies in its layers. Oxidized Tl^{3+} occupies an inner-sphere TCS configuration. Tl sorption onto todorokite, triclinic birnessite (no vacant sites in the layer lattice) or ferrihydrite was observed without thermodynamically unfavored oxidation. Tl^+ is enriched through outer-sphere surface adsorption in the interlayers and the tunnel center in these Mn minerals [118,127,190]. For layered vernadite, low dissolved Tl concentrations dictate higher TCS oxidative enrichment and vice versa. Studies have shown that Tl enrichments were adsorbed exclusively as Tl^{3+} at a low Tl/Mn ratio of 0.02, while a high Tl/Mn ratio of 0.127 has shown that more than 50% of Tl was sorbed as Tl^+. This was interpreted to be a result of blockades and complete uptake of the vacant sites. Excessive critical metals without adequate vacant sites to sorb onto tend to be non-oxidatively adsorbed, either in the loose-bound interlayers or edge-sharing configurations [62,122,123,190]. This is also implicative of the micro-enrichment mechanisms of other critical metals. In addition to Tl lattice oxidative incorporations, the formation of independent Tl_2O_3 particles on the Fe-Mn surface at high Tl loadings was also observed, corresponded with the decrease in the signature peak of vernadite 7.2-Å. This also suggests the gradual uptake of Tl has been accompanied by the dissolution/substitution of the Mn oxides [118,189]. Manceau et al. [127] also supplemented another possible mechanism for Tl concentration. Their work suggested that the incomplete oxidative enrichment of Tl^+ cannot be simply explained by the saturation of Mn vacancy caused by the excessive Tl, but that a partial fraction of Tl^+ would be sorbed on the crystallographic site of Ba at the surface of the Mn layers, which is analogous to the surface site of K which is also suitable for Tl sorption.

5.4.3. Selenium

Although selenium in Fe-Mn crusts is also enriched more than 100 times compared to the Earth's crust value, studies regarding Se adsorption in Fe-Mn deposits have been limited [42]. Se in Fe-Mn nodules has an enrichment range of 1.78–6.88 ppm, whereas Se in crusts shows 3.95–8.82 ppm [72]. Se also shows a relatively high content of 14.8 ppm in the PPCZ Fe-Mn crusts [2]. Selenium contents are depleted in the surface water and increase with water depths and demonstrates a relatively constant concentration for adsorption at typical Fe-Mn crust and nodule precipitation depths [72,191]. Se in modern seawater consists of mainly Se(VI) and Se(IV), in the forms of SeO_4^{2-} and SeO_3^{2-} in seawater pH conditions [60], but selenate Se(VI) is the predominate species in oxic seawater due to the higher solubility [187,191]. The negatively charged Se species tend to bind on the positively charged FeOOH [33], which is in good agreement with correlation analysis which suggested a positive Se-Fe association [72,187]. Previous sorption experiments showed that δ-MnO_2 and amorphous FeOOH separately exhibit preferential adsorption to Se(IV) and Se(VI), indicating an oxidative enrichment by Mn phase and structural incorporation by Fe phase. However, Fe phase shows a much larger efficiency to adsorb Se than Mn phase (26.4 mg/L of Fe displayed the same Se sorption ability as 100 mg/L of Mn), which reveals that Se is predominantly adsorbed by amorphous FeOOH [145]. Hence, the combination of this evidence indicates that Se is predominately enriched in the Fe-Mn deposits by the adsorption of Se onto the Fe oxyhydroxide particles [33,72,145].

5.4.4. Cadmium

Cd(II) as a single-valent heavy metal is often discussed with similar transitional elements like Cu and Ni [192–194]. However, many Cd studies regarding enrichments on δ-MnO_2 and FeOOH are from environmental perspectives instead of the enrichment study of marine Fe-Mn crusts and nodules. Hence, Cd enrichment research in marine Fe-Mn deposits is limited. Cd is more enriched in nodules with higher diagenetic influences (2.7–25.2 ppm) than pure hydrogenetic crusts (1.93–4.11 ppm) [2,72], and also showed an evident increase with deeper depths [72,88,195]. Unlike previous dispersed elements, Cd demonstrates moderately balanced speciation, i.e., $CdCl^+$ (36%), $CdCl_2$ (45%)

and $CdCl_3^-$ (16%) [60,184], therefore, Cd electro-preferences dictate that Cd should be adsorbed on both Mn and Fe phases, as supported by leaching results [33]. Sorption experiments also elaborated on the preferential uptake of Cd in layered MnO_2 rather than ferrihydrite [106,131], as suggested by correlation analysis [72]. Cd in hydrogenetic environments has shown a high preference to sorb onto layer vacancies in TCS coordination, only showing DES/DCS coordination modes upon reducing conditions, i.e., being driven out of the layer vacancy to edge sites [106,125,193], but due to the large radius of Cd^{2+} (1.09-Å), Cd incorporation into the Mn layers is likely limited. Under diagenetic conditions, todorokite preferentially incorporates Cd in its tunnel structure and Cd is mobilized from the sediment during early diagenesis, which controls significant Cd enrichment in diagenetic nodules [2,105]. Randall et al. [196] examined Cd coordination in a similar tunneled mineral, cryptomelane, and suggested hydrated tunnel-center occupation through replacing H^+ and possible TCS to the tunnel wall, which is implicative of this issue.

5.5. Other Critical Elements

5.5.1. Lithium

Li enrichments have shown affinities to geneses in the order of hydrogenetic < phosphatized < diagenetic < hydrothermal. Li contents in marine Fe-Mn deposits may reach up to more than 300 ppm in diagenetic nodules but exhibit much lower contents in hydrogenetic crusts and nodules (2.92 ppm). Some hydrothermal samples could uniquely stimulate higher Li contents over 800 ppm [2,197,198]. Sequential leaching and correlation analysis indicated that Li should be largely associated with the aluminosilicate phase and δ-MnO_2. Coefficients between Li and Al, Mn, Fe, Si were 0.98, 0.94, 0.07 and 0.89, suggesting that lithium is present mostly in the aluminosilicate phase and partly Mn phase rather than in other phases [33,38,199]. Feng et al. [200] have shown that Li in hydrogenetic layered MnO_2 is adsorbed in the outer-sphere hydrated interlayer. Jiang et al. [38] have suggested that Li incorporation in diagenetic 10-Å manganate mainly occupies the tunnel-wall sites in the 3-D tunnel. However, the large ionic radius and the low oxidation valence of Li make it inferior in compensating the structural charge deficit and would relatively limit its enrichment. In addition, hydrogenetic layered MnO_2 can hardly adsorb Li^+ into its structure because of the lack of available sites and large radius difference [112]. Despite high Li contents, the investigations regarding Li enrichments have been few and dissatisfactory in elaborating on the high Li enrichments in Fe-Mn nodules [33,38,199]. The current research status of Li in marine Fe-Mn crusts and nodules requires continuous studies.

5.5.2. Molybdenum, Tungsten and Vanadium

Mo, W and V are generally enriched in hydrogenetic, diagenetic and mixed hydrogenetic–diagenetic geneses of deep-sea Fe-Mn crusts and nodules, their concentrations do not differ significantly under diagenetic or hydrogenetic conditions (Table 1) [2,37] and their contents only alter slightly even in the phosphatized Fe-Mn crusts [4,92,102]. Mo and V contents in hydrogenetic and diagenetic samples range from 400 to 700 ppm, while W contents are much lower, typically ranging below 100 ppm. The extremely low seawater V concentration (53–60 pmol/L), 1/1800 of the seawater Mo concentration, also reflects the high V adsorption proficiency and higher V enrichment factor in marine Fe-Mn crusts and nodules [2,201]. In the oxic oceanic environment, Mo and W are mostly present as Mo^{6+} and W^{6+}, while V exists exclusively as V^{5+}. Their seawater species are mainly tetrahedral anion complexes, MoO_4^{2-}, WO_4^{2-} and VO_4^{3-}, which all can be progressively enriched on Fe-Mn (oxy)hydroxides. Thus, the oxidative reactions are less observed with Mo and W in Fe-Mn crusts and nodules despite their multi-valent properties [60]. Their electro-complexions direct their preferential sorption onto Fe oxyhydroxides as supported by the leaching results that showed Mo and W are dominantly distributed in Fe phase. However, in situ mappings and correlation analysis also revealed high Mo and W distributions and host phases in the Mn oxides, thus, similar to platinum, a similar process of overcoming the electro-repulsion might be in effect for Mo and W enrichments [37,202]. Vanadium, on the

other hand, shows balanced positive and negative species that interact with both Mn and Fe phases, hence justifying the combined Mn and Fe phase enrichments and the positive V-Mn and V-Fe correlations [31,63,203]. Extensive XAS results and geometry modeling have explained that the coordination preferences, generally speaking, of Mo W and V, all form inner-sphere surface complexes on δ-MnO_2 and FeOOH surfaces mainly through DCS and DES configurations on the margins or rims of the MnO_6 and FeO_6 layers [63,132,204,205]. Mo, W and V distortions from tetrahedral to octahedral units upon surface complexations were commonly detected for δ-MnO_2 and partially detected for ferrihydrite in hydrogenetic nodules. The metal symmetric changes are suggested to be driven by the formation of inner-sphere complexes on specific sites of the oxide surface [37,202]. It was suggested that W species were distorted on both Mn and Fe oxides through DCS and DES coordination modes [37,132]. For Mo, no distortion and only a few corner-sharing complexes were observed when interacting with Fe oxyhydroxides and most Mo enriched in Mn phase was distorted to octahedral MoO_6 units [133,202,204,205]. For V, adsorption occurs by the formation of inner-sphere surface complexes resulting from corner-sharing complexes between VO_4^{3-} and FeO_6 and MnO_6 units, and edge-sharing mode is not energetically favored for V [63,206].

5.5.3. Titanium

The Ti contents in marine ferromanganese crusts are as exceptionally high as 1.7%, but Ti experiences significant depletion under phosphatization (Figure 5) [92,102]. Despite the high Ti contents in hydrogenetic Fe-Mn crusts, the Ti enrichment factor is less impressive because Ti in the Earth's crust is also as high as 4000 ppm [50]. The high titanium concentration is well known for its almost exclusive positive association with Fe phases under hydrogenetic conditions [32,33]. The highly positive Ti-Fe correlation was interpreted as hydrated TiO_2 being intergrown in the amorphous FeOOH structures, and previous observation has found in situ Ti precipitates associated with Fe-rich areas [32,128,207]. The high titanium contents and the associative distribution with Fe phase are considered indicators for pure hydrogenetic conditions as revealed by TEM and the phase distribution [25,207]. Diagenetic inputs and phosphatization markedly affect the Ti phase distribution and contents, and highly phosphatized crusts demonstrate evident Ti content release and Ti host-phase transfer. Leaching results revealed that up to 30% of Ti was remobilized to the residue phase from Fe phase in the phosphatized Fe-Mn crust layers, while the reductive dissolution of Ti-hosting Fe oxyhydroxides leads to large intergrown-Ti releases [25,35,208]. Titanium, as a crucial critical metal highly enriched in marine Fe-Mn crusts, is relatively lacking in current research compared to its importance and high enrichment in Fe-Mn crusts, requiring further studies.

5.5.4. Antimony and Arsenic

Multi-valent As and Sb are highly enriched in the oceanic Fe-Mn crusts and nodules, they are commonly distributed in natural systems and reservoirs [2,209]. There is currently only limited research explaining As and Sb enrichments in natural marine Fe-Mn crusts and nodules. However, As and Sb have been pervasively investigated from environmental perspectives and analyzed through sorption simulations on δ-MnO2 and ferrihydrite/goethite, which have shown bountiful implications regarding As and Sb enrichments [135,136,138,141,210]. As and Sb in Fe-Mn crusts from the PCZ showed values of 393 ppm and 39.3 ppm, whereas diagenetic nodules from the Peru Basin showed 65 ppm and 61 ppm [2,42]. Sb is more correlated to Mn and As is more correlated to Fe, and increasing Mn/Fe conditions are associated with higher Sb and lower As concentrations, which explain their separate affiliations towards diagenetic and hydrogenetic influences [134,211]. Early studies showed that they were nearly all pentavalent in marine Fe-Mn oxides and mainly enriched in amorphous Fe oxyhydroxides through sorption experiments and sequential leaching [33,60,211,212]. However, many studies have also found and advocated feasible As and Sb oxidative enrichments on hydrogenetic δ-MnO2 [135,137,141,210]. Qin

et al. [134] observed evident As and Sb enrichments onto δ-MnO2. Mn phase contributes 14% to 29% Sb enrichment in hydrogenetic conditions and 27% to 54% Sb enrichment in diagenetic conditions. The same trends were also observed for As. Trivalent and pentavalent As and Sb exhibit different sorption behaviors, as As(III) and Sb(III) are predominately accumulated on the surface of Mn oxides through oxidative complexations, whereas As(V) and Sb(V) were suggested to be enriched on ferrihydrites and goethite through inner-sphere structural incorporations and co-precipitations [137–139,143,213]. Previous sorption results revealed that only 10% of seawater As(V) and Sb(V) were enriched onto the Mn oxides, whereas the majority of As(V) and Sb(V) are enriched through structural incorporations on the Fe oxyhydroxides without the occurrence of oxidation of trivalent As and Sb on Fe phase [140,212,214]. This suggested the separate roles of Mn and Fe phases in enriching As and Sb, that Mn phase likely adsorbs more low-valent species through oxidative enrichments and Fe phase likely adsorbs more higher-valent species through structural incorporations [136,142]. Extensive XAS investigations on As and Sb coordination analysis showed that As and Sb mainly occupy DCS and DES configurations [134,142]. Due to their geometric differences, $Sb(OH)_6^-$ is inclined to form DES complexes because of its octahedral similarity with MnO_6 units, whereas tetrahedral AsO_4^{3-} struggles to bind with MnO_6 units laterally, hence, a DCS complex is preferred [134,210,215].

6. Conclusions and Summary

Marine Fe-Mn Co-rich crusts and polymetallic nodules are salient deep-sea mineral deposits that enrich large quantities of critical metals. Revealing the occurrence states, enrichment processes and mechanisms of these critical metals in Fe-Mn crusts and nodules is paramount to understanding the extreme enrichments of critical elements in marine Fe-Mn deposits, evaluating the resource potentials in Fe-Mn crusts and nodules and guiding the exploitations and prospecting of their metal resources. This study systematically reviews and elucidates the progress and findings regarding the critical metal research in crusts and nodules of recent years and obtains major understandings as follows:

The influencing factors of critical metal enrichments in crusts and nodules are chiefly: the growth rates, water depth variations, electro-chemical speciation, post-depositional phosphatization and the structures of the Fe-Mn adsorbents. The effects of these factors greatly influence critical metal enrichments and their geochemical behaviors during the enrichments in Fe-Mn crusts and nodules.

Five major enrichment pathways in Fe-Mn (oxy)hydroxides are concluded: (1) Ni, Cu, Zn and Li are enriched through direct complexations on the Mn oxides; (2) Co, Ce and Tl are enriched mainly through oxidation–substitution on the Mn oxides; (3) REY (except for Ce), Cd, Mo, W and V are partitioned between Fe and Mn (oxy)hydroxides through electro-attractiveness and overcoming repulsions; (4) seawater anionic Te, Pt, As and Sb show trends that their low-valence species are oxidatively enriched on δ-MnO_2, in addition to the electro-driven adsorption onto FeOOH, while high-valence species are likely structurally incorporated in amorphous FeOOH to exhibit combined Mn-Fe phase enrichments; (5) Ti and Se show predominant sorption by amorphous FeOOH.

There are primarily four coordination preferences of enriched critical metals in layered and tunneled Mn oxides: (1) incorporations into the layers/tunnel walls are common for Co, Ni and Cu; (2) triple corner-sharing (TCS) complexes are common for Co, Ni, Cu, Zn and Tl, double corner-sharing (DCS) complexes are common for As, Sb, Mo, W, V and Te; (3) edge-sharing complexes are common for the corner-sharing metals when they are less competitive to take up corner-sharing positions or in less oxidizing conditions when the metals are less able to react with layer vacancies; (4) adsorbed in hydrated loosely bound interlayers which are common for low-electro-charge metal species like Li^+ and Tl^+ as well as electro-compensating elements.

Major ore-forming elements (Co, Ni, Cu and Zn), REY, PGE, dispersed elements (Te, Tl, Se and Cd) and other enriched critical metals (Mo, W, V, Li and Ti) in crusts and nodules demonstrate vastly varied enrichment behaviors. In our discussion of the

critical metal enrichments, critical metals generally exhibit a dominant association with the Mn oxides or Fe oxyhydroxide and show an enrichment preference for diagenetic or hydrogenetic conditions. Critical metals are progressively accumulated through surface complexation and substitution in the structure of Fe-Mn (oxy)hydroxides with respect to micro-uptake perspectives. Their unique enrichment characteristics, enrichment processes and mechanisms under different geneses and oceanic conditions contribute to forming the extreme enrichments of critical metal abundance in Fe-Mn nodules and crusts. This study provides a conclusive view to understanding the geochemical behavior of critical metals in oceanic environments and bears significance to direct further exploration of critical metals in oceanic Fe-Mn crusts and nodules.

References

1. Lusty, P.A.J.; Murton, B.J. Deep-Ocean Mineral Deposits: Metal Resources and Windows into Earth Processes. *Elements* **2018**, *14*, 301–306. [CrossRef]
2. Hein, J.R.; Koschinsky, A. Deep-Ocean Ferromanganese Crusts and Nodules. In *Treatise on Geochemistry*; Elsevier: Amsterdam, The Netherlands, 2014; pp. 273–291.
3. Hein, J.R.; Koschinsky, A.; Kuhn, T. Deep-ocean polymetallic nodules as a resource for critical materials. *Nat. Rev. Earth Environ.* **2020**, *1*, 158–169. [CrossRef]
4. Halbach, P.; Jahn, A.; Cherkashov, G. *Marine Co-Rich Ferromanganese Crust Deposits: Description and Formation, Occurrences and Distribution, Estimated World-Wide Resources*; Springer: Cham, Switzerland, 2017; pp. 65–141.
5. Kuhn, T.; Wegorzewski, A.; Ruehlemann, C.; Vink, A. *Composition, Formation, and Occurrence of Polymetallic Nodules*; Springer: Cham, Switzerland, 2017; pp. 23–63.
6. Wegorzewski, A.V.; Kuhn, T. The influence of suboxic diagenesis on the formation of manganese nodules in the Clarion Clipperton nodule belt of the Pacific Ocean. *Mar. Geol.* **2014**, *357*, 123–138. [CrossRef]
7. Halbach, P. Processes controlling the heavy-metal distribution in pacific ferromanganese nodules and crusts. *Geol. Rundsch.* **1986**, *75*, 235–247. [CrossRef]
8. Marino, E.; Gonzalez, F.J.; Lunar, R.; Reyes, J.; Medialdea, T.; Castillo-Carrion, M.; Bellido, E.; Somoza, L. High-Resolution Analysis of Critical Minerals and Elements in Fe-Mn Crusts from the Canary Island Seamount Province (Atlantic Ocean). *Minerals* **2018**, *8*, 285. [CrossRef]
9. Hein, J.R.; Koschinsky, A.; Bau, M.; Manheim, F.; Kang, J.-K.; Roberts, L. *Cobalt-Rich Ferromanganese Crusts in the Pacific*; CRC Press: Boca Raton, FL, USA, 2000; Volume 17, pp. 239–279.
10. Sutherland, K.M.; Wankel, S.D.; Hein, J.R.; Hansel, C.M. Spectroscopic Insights Into Ferromanganese Crust Formation and Diagenesis. *Geochem. Geophys. Geosystems* **2020**, *21*, e2020GC009074. [CrossRef]
11. Li, Y.H.; Schoonmaker, J.E. Chemical Composition and Mineralogy of Marine Sediments. In *Treatise on Geochemistry*, 2nd ed.; Holland, H.D., Turekian, K.K., Eds.; Elsevier: Oxford, UK, 2014; pp. 1–32.
12. Manceau, A.; Lanson, M.; Takahashi, Y. Mineralogy and crystal chemistry of Mn, Fe, Co, Ni, and Cu in a deep-sea Pacific polymetallic nodule. *Am. Mineral.* **2014**, *99*, 2068–2083. [CrossRef]
13. Kwon, K.D.; Refson, K.; Sposito, G. Understanding the trends in transition metal sorption by vacancy sites in birnessite. *Geochim. Et Cosmochim. Acta* **2013**, *101*, 222–232. [CrossRef]
14. Bodei, S.; Manceau, A.; Geoffroy, N.; Baronnet, A.; Buatier, M. Formation of todorokite from vernadite in Ni-rich hemipelagic sediments. *Geochim. Et Cosmochim. Acta* **2007**, *71*, 5698–5716. [CrossRef]
15. Manceau, A.; Drits, V.A.; Silvester, E.; Bartoli, C.; Lanson, B. Structural mechanism of Co^{2+} oxidation by the phyllomanganate buserite. *Am. Mineral.* **1997**, *82*, 1150–1175. [CrossRef]
16. Lee, S.; Xu, H.F.; Xu, W.Q.; Sun, X.M. The structure and crystal chemistry of vernadite in ferromanganese crusts. *Acta Crystallogr. Sect. B-Struct. Sci. Cryst. Eng. Mater.* **2019**, *75*, 591–598. [CrossRef]
17. U.S.G.S. *Mineral Commodity Summaries 2023*; U.S. Geological Survey: Reston, VA, USA, 2023.

18. Wang, D. Study on critical mineral resources: Significance of research, determination of types, attributes of resources, progress of prospecting, problems of utilization, and direction of exploitation. *Acta Geol. Sin.* **2019**, *93*, 1189–1209.

19. U.S. Department of Commerce. *A Federal Strategy to Ensure Secure and Reliable Supplies of Critical Minerals*; U.S. Department of Commerce: Washington, DC, USA, 2019.

20. Takahashi, Y.; Manceau, A.; Geoffroy, N.; Marcus, M.A.; Usui, A. Chemical and structural control of the partitioning of Co, Ce, and Pb in marine ferromanganese oxides. *Geochim. Et Cosmochim. Acta* **2007**, *71*, 984–1008. [CrossRef]

21. Peacock, C.L.; Sherman, D.M. Crystal-chemistry of Ni in marine ferromanganese crusts and nodules. *Am. Mineral.* **2007**, *92*, 1087–1092. [CrossRef]

22. Usui, A. Nickel and copper accumulation as essential elements in 10-Å manganite of deep-sea manganese nodules. *Nature* **1979**, *279*, 411–413. [CrossRef] [PubMed]

23. Elderfield, H.; Hawkesworth, C.J.; Greaves, M.J.; Calvert, S.E. Rare-earth element geochemistry of oceanic ferromanganese nodules and associated sediments. *Geochim. Et Cosmochim. Acta* **1981**, *45*, 513–528. [CrossRef]

24. Ohta, A.; Kawabe, I. REE(III) adsorption onto Mn dioxide (δ-MnO_2) and Fe oxyhydroxide: Ce(III) oxidation by δ-MnO_2. *Geochim. Et Cosmochim. Acta* **2001**, *65*, 695–703. [CrossRef]

25. Bau, M.; Koschinsky, A.; Dulski, P.; Hein, J.R. Comparison of the partitioning behaviours of yttrium, rare earth elements, and titanium between hydrogenetic marine ferromanganese crusts and seawater. *Geochim. Et Cosmochim. Acta* **1996**, *60*, 1709–1725. [CrossRef]

26. Hein, J.R.; Koschinsky, A.; Halliday, A.N. Global occurrence of tellurium-rich ferromanganese crusts and a model for the enrichment of tellurium. *Geochim. Et Cosmochim. Acta* **2003**, *67*, 1117–1127. [CrossRef]

27. Hein, J.R.; Spinardi, F.; Okamoto, N.; Mizell, K.; Thorburn, D.; Tawake, A. Critical metals in manganese nodules from the Cook Islands EEZ, abundances and distributions. *Ore Geol. Rev.* **2015**, *68*, 97–116. [CrossRef]

28. Marino, E.; González, F.J.; Somoza, L.; Lunar, R.; Ortega, L.; Vázquez, J.T.; Reyes, J.; Bellido, E. Strategic and rare elements in Cretaceous-Cenozoic cobalt-rich ferromanganese crusts from seamounts in the Canary Island Seamount Province (northeastern tropical Atlantic). *Ore Geol. Rev.* **2017**, *87*, 41–61. [CrossRef]

29. Hein, J.R.; Konstantinova, N.; Mikesell, M.; Mizell, K.; Fitzsimmons, J.N.; Lam, P.J.; Jensen, L.T.; Xiang, Y.; Gartman, A.; Cherkashov, G.; et al. Arctic Deep Water Ferromanganese-Oxide Deposits Reflect the Unique Characteristics of the Arctic Ocean. *Geochem. Geophys. Geosystems* **2017**, *18*, 3771–3800. [CrossRef]

30. Muiños, S.B.; Hein, J.R.; Frank, M.; Monteiro, J.H.; Gaspar, L.; Conrad, T.; Pereira, H.G.; Abrantes, F. Deep-sea Fe-Mn Crusts from the Northeast Atlantic Ocean: Composition and Resource Considerations. *Mar. Georesources Geotechnol.* **2013**, *31*, 40–70. [CrossRef]

31. Koschinsky, A.; Hein, J.R.; Kraemer, D.; Foster, A.L.; Kuhn, T.; Halbach, P. Platinum enrichment and phase associations in marine ferromanganese crusts and nodules based on a multi-method approach. *Chem. Geol.* **2020**, *539*, 119426. [CrossRef]

32. Koschinsky, A.; Halbach, P. Sequential leaching of marine ferromanganese precipitates: Genetic implications. *Geochim. Et Cosmochim. Acta* **1995**, *59*, 5113–5132. [CrossRef]

33. Koschinsky, A.; Hein, J.R. Uptake of elements from seawater by ferromanganese crusts: Solid-phase associations and seawater speciation. *Mar. Geol.* **2003**, *198*, 331–351. [CrossRef]

34. Kashiwabara, T.; Oishi, Y.; Sakaguchi, A.; Sugiyama, T.; Usui, A.; Takahashi, Y. Chemical processes for the extreme enrichment of tellurium into marine ferromanganese oxides. *Geochim. Et Cosmochim. Acta* **2014**, *131*, 150–163. [CrossRef]

35. Kuhn, T.; Bostick, B.C.; Koschinsky, A.; Halbach, P.; Fendorf, S. Enrichment of Mo in hydrothermal Mn precipitates: Possible Mo sources, formation process and phase associations. *Chem. Geol.* **2003**, *199*, 29–43. [CrossRef]

36. Wegorzewski, A.V.; Grangeon, S.; Webb, S.M.; Heller, C.; Kuhn, T. Mineralogical transformations in polymetallic nodules and the change of Ni, Cu and Co crystal -chemistry upon burial in sediments. *Geochim. Et Cosmochim. Acta* **2020**, *282*, 19–37. [CrossRef]

37. Kashiwabara, T.; Takahashi, Y.; Marcus, M.A.; Uruga, T.; Tanida, H.; Terada, Y.; Usui, A. Tungsten species in natural ferromanganese oxides related to its different behavior from molybdenum in oxic ocean. *Geochim. Et Cosmochim. Acta* **2013**, *106*, 364–378. [CrossRef]

38. Jiang, X.; Lin, X.; Yao, D.; Zhai, S.; Guo, W. Geochemistry of lithium in marine ferromanganese oxide deposits. *Deep. -Sea Res. Part I-Oceanogr. Res. Pap.* **2007**, *54*, 85–98. [CrossRef]

39. Toro, N.; Robles, P.; Jeldres, R.I. Seabed mineral resources, an alternative for the future of renewable energy: A critical review. *Ore Geol. Rev.* **2020**, *126*, 103699. [CrossRef]

40. Lusty, P.A.J.; Hein, J.R.; Josso, P. Formation and occurrence of Ferromanganese Crusts: Earth's Storehouse for Critical Metals. *Elements* **2018**, *14*, 313–318. [CrossRef]

41. Hein, J.R.; Conrad, T.A.; Staudigel, H. Seamount mineral deposits: A source of rare metals for high-technology industries. *Oceanography* **2010**, *23*, 184–189. [CrossRef]

42. Hein, J.R.; Mizell, K.; Koschinsky, A.; Conrad, T.A. Deep-ocean mineral deposits as a source of critical metals for high- and green-technology applications: Comparison with land-based resources. *Ore Geol. Rev.* **2013**, *51*, 1–14. [CrossRef]

43. Verlaan, P.A.; Cronan, D.S.; Morgan, C.L. A comparative analysis of compositional variations in and between marine ferromanganese nodules and crusts in the South Pacific and their environmental controls. *Prog. Oceanogr.* **2004**, *63*, 125–158. [CrossRef]

44. Verlaan, P.A.; Cronan, D.S. Origin and variability of resource-grade marine ferromanganese nodules and crusts in the Pacific Ocean: A review of biogeochemical and physical controls. *Geochemistry* **2022**, *82*, 125741. [CrossRef]

45. Usui, A.; Terashima, S. Deposition of hydrogenetic and hydrothermal manganese minerals in the Ogasawara (Bonin) Arc Area, Northwest Pacific. *Mar. Georesources Geotechnol.* **1997**, *15*, 127–154. [CrossRef]

46. Surya Prakash, L.; Ray, D.; Paropkari, A.L.; Mudholkar, A.V.; Satyanarayanan, M.; Sreenivas, B.; Chandrasekharam, D.; Kota, D.; Kamesh Raju, K.A.; Kaisary, S.; et al. Distribution of REEs and yttrium among major geochemical phases of marine Fe–Mn-oxides: Comparative study between hydrogenous and hydrothermal deposits. *Chem. Geol.* **2012**, *312–313*, 127–137. [CrossRef]

47. Kuhn, T.; Bau, M.; Blum, N.; Halbach, P. Origin of negative Ce anomalies in mixed hydrothermal-hydrogenetic Fe-Mn crusts from the Central Indian Ridge. *Earth Planet. Sci. Lett.* **1998**, *163*, 207–220. [CrossRef]

48. Mikhailik, P.E.; Mikhailik, E.V.; Zarubina, N.V.; Blokhin, M.G. Distribution of rare-earth elements and yttrium in hydrothermal sedimentary ferromanganese crusts of the Sea of Japan. *Russ. Geol. Geophys.* **2017**, *58*, 1530–1542. [CrossRef]

49. Pelleter, E.; Fouquet, Y.; Etoubleau, J.; Cheron, S.; Labanieh, S.; Josso, P.; Bollinger, C.; Langlade, J. Ni-Cu-Co-rich hydrothermal manganese mineralization in the Wallis and Futuna back-arc environment (SW Pacific). *Ore Geol. Rev.* **2017**, *87*, 126–146. [CrossRef]

50. Wedepohl, K.H. The Composition Of The Continental-Crust. *Geochim. Et Cosmochim. Acta* **1995**, *59*, 1217–1232. [CrossRef]

51. Fortier, S.M.; Nassar, N.T.; Lederer, G.W.; Brainard, J.; Gambogi, J.; McCullough, E.A. *Draft Critical Mineral List—Summary of Methodology and Background Information—U.S. Geological Survey Technical input Document in Response to Secretarial Order No. 3359*; Open-File Report 2018-1021; U.S. Geological Survey: Reston, VA, USA, 2018; p. 26.

52. Gulley, A.L.; Nassar, N.T.; Xun, S. China, the United States, and competition for resources that enable emerging technologies. *Proc. Natl. Acad. Sci. USA* **2018**, *115*, 4111–4115. [CrossRef]

53. Industrie, D.E.E.; Isi, F. *Critical Raw Materials for the EU—Report of the Ad-hoc Working Group on Defining Critical Raw Materials*; European Commission: Ispra, Italy, 2010.

54. Sovacool, B.K.; Ali, S.H.; Bazilian, M.; Radley, B.; Nemery, B.; Okatz, J.; Mulvaney, D. Sustainable minerals and metals for a low-carbon future. *Science* **2020**, *367*, 30. [CrossRef]

55. Nassar, N.T.; Graedel, T.E.; Harper, E.M. By-product metals are technologically essential but have problematic supply. *Sci. Adv.* **2015**, *1*, e1400180. [CrossRef]

56. Tu, G.C.; Gao, Z.M. Ore-forming mechanism of the Dispersed Elements. *Bull. Chin. Acad. Sci.* **2003**, *5*, 358–361. [CrossRef]

57. Tu, G.C.; Gao, Z.M.; Hu, R.Z.; Zhang, Q.; Li, C.Y.; Zhao, Z.H.; Zhang, B.G. *Geochemistry and Mineralization of the Dispersed Elements*; Science Press: Beijing, China, 2003.

58. Hodkinson, R.A.; Cronan, D.S. Regional and depth variability in the composition of cobalt-rich ferromanganese crusts from the SOPAC area and adjacent parts of the central equatorial Pacific. *Mar. Geol.* **1991**, *98*, 437–447. [CrossRef]

59. Mohwinkel, D.; Kleint, C.; Koschinsky, A. Phase associations and potential selective extraction methods for selected high-tech metals from ferromanganese nodules and crusts with siderophores. *Appl. Geochem.* **2014**, *43*, 13–21. [CrossRef]

60. Byrne, R.H. Inorganic speciation of dissolved elements in seawater: The influence of pH on concentration ratios. *Geochem. Trans.* **2002**, *3*, 11. [CrossRef] [PubMed]

61. Maeno, M.Y.; Ohashi, H.; Yonezu, K.; Miyazaki, A.; Okaue, Y.; Watanabe, K.; Ishida, T.; Tokunaga, M.; Yokoyama, T. Sorption behavior of the Pt(II) complex anion on manganese dioxide (δ-MnO_2): A model reaction to elucidate the mechanism by which Pt is concentrated into a marine ferromanganese crust. *Miner. Depos.* **2016**, *51*, 211–218. [CrossRef]

62. Zhao, H.Y.; Feng, X.H.; Lee, S.S.; Reinhart, B.; Elzinga, E.J. Sorption and oxidation of Co(II) at the surface of birnessite: Impacts of aqueous Mn(II). *Chem. Geol.* **2023**, *618*, 121281. [CrossRef]

63. Zhu, H.W.; Xiao, X.Y.; Guo, Z.H.; Peng, C.; Wang, X.H.; Yang, A.D. Characteristics and behaviour of vanadium(V) adsorption on goethite and birnessite. *Environ. Earth Sci.* **2020**, *79*, 240. [CrossRef]

64. Mitsunobu, S.; Takahashi, Y.; Terada, Y.; Sakata, M. Antimony(V) Incorporation into Synthetic Ferrihydrite, Goethite, and Natural Iron Oxyhydroxides. *Environ. Sci. Technol.* **2010**, *44*, 3712–3718. [CrossRef]

65. Takematsu, N.; Sato, Y.; Okabe, S. Factors controlling the chemical-composition of marine manganese nodules and crusts—A review and synthesis. *Mar. Chem.* **1989**, *26*, 41–56. [CrossRef]

66. Usui, A.; Nishi, K.; Sato, H.; Nakasato, Y.; Thornton, B.; Kashiwabara, T.; Tokumaru, A.; Sakaguchi, A.; Yamaoka, K.; Kato, S.; et al. Continuous growth of hydrogenetic ferromanganese crusts since 17 Myr ago on Takuyo-Daigo Seamount, NW Pacific, at water depths of 800–5500 m. *Ore Geol. Rev.* **2017**, *87*, 71–87. [CrossRef]

67. Halbach, P.; Marbler, H. Marine ferromanganese crusts: Contents, distribution and enrichment of strategic minor and trace elements. In *BGR-Report*; BGR: Berlin, Germany, 2009; pp. 1–73.

68. Halbach, P.; Segl, M.; Puteanus, D.; Mangini, A. Co-fluxes and growth-rates in ferromanganese deposits from central pacific seamount areas. *Nature* **1983**, *304*, 716–719. [CrossRef]

69. Takahashi, Y.; Shimizu, H.; Usui, A.; Kagi, H.; Nomura, M. Direct observation of tetravalent cerium in ferromanganese nodules and crusts by X-ray-absorption near-edge structure (XANES). *Geochim. Et Cosmochim. Acta* **2000**, *64*, 2929–2935. [CrossRef]

70. Manheim, F.T.; Lanebostwick, C.M. Cobalt in ferromanganese crusts as a monitor of hydrothermal discharge on the Pacific sea-floor. *Nature* **1988**, *335*, 59–62. [CrossRef]

71. Puteanus, D.; Halbach, P. Correlation of co concentration and growth-rate—A method for age-determination of ferromanganese crusts. *Chem. Geol.* **1988**, *69*, 73–85. [CrossRef]

72. Fu, Y.Z.; Wen, H.J. Variabilities and enrichment mechanisms of the dispersed elements in marine Fe–Mn deposits from the Pacific Ocean. *Ore Geol. Rev.* **2020**, *121*, 103470. [CrossRef]

73. Conrad, T.; Hein, J.R.; Paytan, A.; Clague, D.A. Formation of Fe-Mn crusts within a continental margin environment. *Ore Geol. Rev.* **2017**, *87*, 25–40. [CrossRef]

74. Guan, Y.; Sun, X.M.; Ren, Y.Z.; Jiang, X.D. Mineralogy, geochemistry and genesis of the polymetallic crusts and nodules from the South China Sea. *Ore Geol. Rev.* **2017**, *89*, 206–227. [CrossRef]

75. Ivanova, Y.M.; Mikhailik, P.E.; Mikhailik, E.V.; Zarubina, N.V.; Blokhin, M.G. Chemical Composition and Genesis of Ferromanganese Crusts from the Sonne Ridge (Kuril Basin, Sea of Okhotsk). *Russ. Geol. Geophys.* **2019**, *60*, 1026–1042. [CrossRef]

76. Douville, E.; Bienvenu, P.; Charlou, J.L.; Donval, J.P.; Fouquet, Y.; Appriou, P.; Gamo, T. Yttrium and rare earth elements in fluids from various deep-sea hydrothermal systems. *Geochim. Et Cosmochim. Acta* **1999**, *63*, 627–643. [CrossRef]

77. Bau, M.; Schmidt, K.; Koschinsky, A.; Hein, J.; Kuhn, T.; Usui, A. Discriminating between different genetic types of marine ferro-manganese crusts and nodules based on rare earth elements and yttrium. *Chem. Geol.* **2014**, *381*, 1–9. [CrossRef]

78. Li, C.; Song, W.; Sun, Z.; Huang, W.; Hu, G.; Yuan, X.; Kao, S.-J. High-Resolution Analysis of Fe-Mn Oxyhydroxide in Ferromanganese Nodules from the Northwestern Pacific Ocean and Insights on Element Mobility. *Minerals* **2023**, *13*, 415. [CrossRef]

79. Ren, J.B.; He, G.W.; Deng, X.G.; Deng, X.Z.; Yang, Y.; Yao, H.Q.; Yang, S.X. Metallogenesis of Co-rich ferromanganese nodules in the northwestern Pacific: Selective enrichment of metallic elements from seawater. *Ore Geol. Rev.* **2022**, *143*, 104778. [CrossRef]

80. Mikhailik, P.E.; Khanchuk, A.I.; Mikhailik, E.V.; Rashidov, V.A.; Savelyev, D.P.; Zarubina, N.V. Ferromanganese Crusts of the North Pacific Ocean. *Russ. J. Pac. Geol.* **2023**, *17*, 101–133. [CrossRef]

81. Yi, L.; Li, Y.; Mikhailik, P.; Qi, Y.; Deng, C. Magnetic and geochemical scanning reveals growth history of marine ferromanganese crust on Detroit Seamount, northwest Pacific since the early Miocene. *Quat. Int.* **2023**, *671*, 52–61. [CrossRef]

82. Halbach, P.; Puteanus, D. The influence of the carbonate dissolution rate on the growth and composition of Co-rich ferromanganese crusts from Central Pacific seamount areas. *Earth Planet. Sci. Lett.* **1984**, *68*, 73–87. [CrossRef]

83. Vonstackelberg, U.; Beiersdorf, H. The formation of manganese nodules between the Clarion and Clipperton fracture-zones southeast of Hawaii. *Mar. Geol.* **1991**, *98*, 411–423. [CrossRef]

84. Jiang, X.; Yao, D.; Zhai, S. Factors controlling the concentration of the transition metals Cu, Co and Ni in the ferromanganese deposits: An overview. *Mar. Geol. Quat. Geol.* **2004**, *24*, 41–48.

85. Hein, J.R.; Schwab, W.C.; Davis, A.S. Cobalt-rich and platinum-rich ferromanganese crusts and associated substrate rocks from the Marshall-islands. *Mar. Geol.* **1988**, *78*, 255–283. [CrossRef]

86. Halbach, P.; Sattler, C.D.; Teichmann, F.; Wahsner, M. Cobalt-rich and platinum-bearing manganese crust deposits on seamounts: Nature, formation, and metal potential. *Mar. Min.* **1989**, *8*, 23–39.

87. Nozaki, Y. Elemental Distribution: Overview. In *Encyclopedia of Ocean Sciences*, 2nd ed.; Steele, J.H., Ed.; Academic Press: Oxford, UK, 2001; pp. 255–260.

88. Hein, J.R.; Conrad, T.A.; Frank, M.; Christl, M.; Sager, W.W. Copper-nickel-rich, amalgamated ferromanganese crust-nodule deposits from Shatsky Rise, NW Pacific. *Geochem. Geophys. Geosystems* **2012**, *13*, Q10022. [CrossRef]

89. De Carlo, E.H.; McMurtry, G.M. Rare-earth element geochemistry of ferromanganese crusts from the Hawaiian Archipelago, central Pacific. *Chem. Geol.* **1992**, *95*, 235–250. [CrossRef]

90. Hein, J.R.; Conrad, T.; Mizell, K.; Banakar, V.K.; Frey, F.A.; Sager, W.W. Controls on ferromanganese crust composition and reconnaissance resource potential, Ninetyeast Ridge, Indian Ocean. *Deep.-Sea Res. Part I-Oceanogr. Res. Pap.* **2016**, *110*, 1–19. [CrossRef]

91. Jiang, X.J.; Lin, X.H.; Yao, D.; Guo, W.D. Enrichment mechanisms of rare earth elements in marine hydrogenetic ferromanganese crusts. *Sci. China-Earth Sci.* **2011**, *54*, 197–203. [CrossRef]

92. Jiang, X.-D.; Sun, X.-M.; Chou, Y.-M.; Hein, J.R.; He, G.-W.; Fu, Y.; Li, D.-f.; Liao, J.-L.; Ren, J.-B. Geochemistry and origins of carbonate fluorapatite in seamount Fe-Mn crusts from the Pacific Ocean. *Mar. Geol.* **2020**, *423*, 106135. [CrossRef]

93. Halbach, P.; Kriete, C.; Prause, B.; Puteanus, D. Mechanisms to explain the platinum concentration in ferromanganese seamount crusts. *Chem. Geol.* **1989**, *76*, 95–106. [CrossRef]

94. Bruland, K.W. Oceanographic distributions of cadmium, zinc, nickel, and copper in the North Pacific. *Earth Planet. Sci. Lett.* **1980**, *47*, 176–198. [CrossRef]

95. Varghese, S.; Ramesh, R.P.; Pillai, R.; Joseph, S.R.; Gopakumar, B.; Sathikumar, R.; Joshi, R.K.; Guha, P.D.; Manoj, R.V.; Nagasundaram, M. Accumulation and enrichment of platinum group elements in hydrogenous Fe-Mn crust and nodules from the Andaman Sea, India. *Curr. Sci.* **2021**, *120*, 1740–1748. [CrossRef]

96. Savelyev, D.P.; Khanchuk, A.I.; Savelyeva, O.L.; Moskaleva, S.V.; Mikhailik, P.E. First Find of Platinum in Cosmogenic Spherules of Ferromanganese Crusts (Fedorov Guyot, Magellan Seamounts, Pacific Ocean). *Dokl. Earth Sci.* **2020**, *491*, 199–203. [CrossRef]

97. Koschinsky, A.; Stascheit, A.; Bau, M.; Halbach, P. Effects of phosphatization on the geochemical and mineralogical composition of marine ferromanganese crusts. *Geochim. Et Cosmochim. Acta* **1997**, *61*, 4079–4094. [CrossRef]

98. Hein, J.R.; Yeh, H.W.; Gunn, S.H.; Sliter, W.V.; Benninger, L.M.; Wang, C.H. Two Major Cenozoic Episodes of Phosphogenesis Recorded in Equatorial Pacific Seamount Deposits. *Paleoceanography* **1993**, *8*, 293–311. [CrossRef]

99. Cui, Y.C.; Shi, X.F.; Liu, J.H.; Ren, X.W. Effects of Phosphatization on the Elemental Association of Cobalt-Rich Crusts. *Geol. Sci. Techology Inf.* **2008**, *27*, 61–67.

100. Ren, X.W.; Liu, J.H.; Chui, Y.C.; Shi, X.F.; Yin, J.W. Effects of phosphatization on enrichment of cobalt in the Co-rich Fe-Mn crusts from seamount MP2 of the Line islands in the Central Pacific. *Adv. Mar. Sci.* **2011**, *29*, 324–329.

101. Pan, J.; De Carlo, E.H.; Liu, S. Effect of phosphatization on element concentration of cobalt-rich ferromanganese crusts. In Proceedings of the ISOPE Ocean Mining Symposium, Seoul, Republic of Korea, 15–19 September 2003; pp. 20–26.

102. Josso, P.; Lusty, P.; Chenery, S.; Murton, B. Controls on metal enrichment in ferromanganese crusts: Temporal changes in oceanic metal flux or phosphatisation? *Geochim. Et Cosmochim. Acta* **2021**, *308*, 60–74. [CrossRef]

103. Oldham, V.E.; Jones, M.R.; Tebo, B.M.; Luther, G.W. Oxidative and reductive processes contributing to manganese cycling at oxic-anoxic interfaces. *Mar. Chem.* **2017**, *195*, 122–128. [CrossRef]

104. Baturin, G.N.; Yushina, I.G. Rare earth elements in phosphate-ferromanganese crusts on Pacific seamounts. *Lithol. Miner. Resour.* **2007**, *42*, 101–117. [CrossRef]

105. Kim, J.; Kwon, K.D. Tunnel cation and water structures of todorokite: Insights into metal partitioning and isotopic fractionation. *Geochim. Et Cosmochim. Acta* **2022**, *333*, 153–165. [CrossRef]

106. van Genuchten, C.M.; Pena, J. Sorption selectivity of birnessite particle edges: A d-PDF analysis of Cd(II) and Pb(II) sorption by δ-MnO_2 and ferrihydrite. *Environ. Sci.-Process. Impacts* **2016**, *18*, 1030–1041. [CrossRef]

107. Wegorzewski, A.V.; Kuhn, T.; Dohrmann, R.; Wirth, R.; Grangeon, S. Mineralogical characterization of individual growth structures of Mn-nodules with different Ni+Cu content from the central Pacific Ocean. *Am. Mineral.* **2015**, *100*, 2497–2508. [CrossRef]

108. Post, J.E.; McKeown, D.A.; Heaney, P.J. Raman spectroscopy study of manganese oxides: Tunnel structures. *Am. Mineral.* **2020**, *105*, 1175–1190. [CrossRef]

109. Post, J.E.; McKeown, D.A.; Heaney, P.J. Raman spectroscopy study of manganese oxides: Layer structures. *Am. Mineral.* **2021**, *106*, 351–366. [CrossRef]

110. Hens, T.; Brugger, J.; Etschmann, B.; Paterson, D.; Brand, H.E.A.; Whitworth, A.; Frierdich, A.J. Nickel exchange between aqueous Ni(II) and deep-sea ferromanganese nodules and crusts. *Chem. Geol.* **2019**, *528*, 119276. [CrossRef]

111. Grangeon, S.; Lanson, B.; Lanson, M. Solid-state transformation of nanocrystalline phyllomanganate into tectomanganate: Influence of initial layer and interlayer structure. *Acta Crystallogr. Sect. B Struct. Sci. Cryst. Eng. Mater.* **2014**, *70*, 828–838. [CrossRef]

112. Zhu, M.; Ginder-Vogel, M.; Sparks, D.L. Cation Effects on the Layer Structure of Biogenic Mn-Oxides. *Environ. Sci. Technol.* **2010**, *44*, 4465–4471. [CrossRef]

113. Yang, P.; Lee, S.; Post, J.E.; Xu, H.; Wang, Q.; Xu, W.; Zhu, M. Trivalent manganese on vacancies triggers rapid transformation of layered to tunneled manganese oxides (TMOs): Implications for occurrence of TMOs in low-temperature environment. *Geochim. Et Cosmochim. Acta* **2018**, *240*, 173–190. [CrossRef]

114. Tournassat, C.; Charlet, L.; Bosbach, D.; Manceau, A. Arsenic(III) Oxidation by Birnessite and Precipitation of Manganese(II) Arsenate. *Environ. Sci. Technol.* **2002**, *36*, 493–500. [CrossRef] [PubMed]

115. Manceau, A.; Steinmann, S.N. Nature of High- and Low-Affinity Metal Surface Sites on Birnessite Nanosheets. *ACS Earth Space Chem.* **2021**, *5*, 66–76. [CrossRef]

116. Grangeon, S.; Fernandez-Martinez, A.; Claret, F.; Marty, N.; Tournassat, C.; Warmont, F.; Gloter, A. In-situ determination of the kinetics and mechanisms of nickel adsorption by nanocrystalline vernadite. *Chem. Geol.* **2017**, *459*, 24–31. [CrossRef]

117. Sherman, D.M.; Peacock, C.L. Surface complexation of Cu on birnessite (δ-MnO_2): Controls on Cu in the deep ocean. *Geochim. Et Cosmochim. Acta* **2010**, *74*, 6721–6730. [CrossRef]

118. Cruz-Hernandez, Y.; Villalobos, M.; Marcus, M.A.; Pi-Puig, T.; Zanella, R.; Martinez-Villegas, N. Tl(I) sorption behavior on birnessite and its implications for mineral structural changes. *Geochim. Et Cosmochim. Acta* **2019**, *248*, 356–369. [CrossRef]

119. Atkins, A.L.; Shaw, S.; Peacock, C.L. Release of Ni from birnessite during transformation of birnessite to todorokite: Implications for Ni cycling in marine sediments. *Geochim. Et Cosmochim. Acta* **2016**, *189*, 158–183. [CrossRef]

120. Simanova, A.A.; Peña, J. Time-Resolved Investigation of Cobalt Oxidation by Mn(III)-Rich δ-MnO2 Using Quick X-ray Absorption Spectroscopy. *Environ. Sci. Technol.* **2015**, *49*, 10867–10876. [CrossRef]

121. Peña, J.; Kwon, K.D.; Refson, K.; Bargar, J.R.; Sposito, G. Mechanisms of nickel sorption by a bacteriogenic birnessite. *Geochimica Et Cosmochimica Acta* **2010**, *74*, 3076–3089. [CrossRef]

122. Simanova, A.A.; Kwon, K.D.; Bone, S.E.; Bargar, J.R.; Refson, K.; Sposito, G.; Peña, J. Probing the sorption reactivity of the edge surfaces in birnessite nanoparticles using nickel(II). *Geochim. Et Cosmochim. Acta* **2015**, *164*, 191–204. [CrossRef]

123. Wick, S.; Pena, J.; Voegelin, A. Thallium Sorption onto Manganese Oxides. *Environ. Sci. Technol.* **2019**, *53*, 13168–13178. [CrossRef]

124. Peña, J.; Bargar, J.R.; Sposito, G. Copper sorption by the edge surfaces of synthetic birnessite nanoparticles. *Chem. Geol.* **2015**, *396*, 196–207. [CrossRef]

125. Sun, Q.; Cui, P.-X.; Zhu, M.; Fan, T.-T.; Ata-Ul-Karim, S.T.; Gu, J.-H.; Wu, S.; Zhou, D.-M.; Wang, Y.-J. Cd(II) retention and remobilization on δ-MnO2 and Mn(III)-rich δ-MnO_2 affected by Mn(II). *Environ. Int.* **2019**, *130*, 104932. [CrossRef] [PubMed]

126. Wang, Z.; Peacock, C.; Kwon, K.D.; Gu, X.; Feng, X.; Li, W. Site-specific isotope fractionation during Zn adsorption onto birnessite: Insights from X-ray absorption spectroscopy, density functional theory and surface complexation modeling. *Geochim. Et Cosmochim. Acta* **2023**, *348*, 68–84. [CrossRef]

127. Manceau, A.; Simionovici, A.; Findling, N.; Glatzel, P.; Detlefs, B.; Wegorzewski, A.V.; Mizell, K.; Hein, J.R.; Koschinsky, A. Crystal Chemistry of Thallium in Marine Ferromanganese Deposits. *ACS Earth Space Chem.* **2022**, *6*, 1269–1285. [CrossRef]

128. Huang, W.; Hu, B.; Song, W.; Zhao, J.; Lu, J.; Meng, X.; Jiang, Y.; Cui, R.; Ding, X. Enrichment and constraints of critical metals in ferromanganese crusts from 13°20′ N seamount of the southern Kyushu-Palau Ridge. *Mar. Geol. Quat. Geol.* **2022**, *42*, 137–148.

129. Ren, Y.; Sun, X.; Guan, Y.; Xiao, Z.; Liu, Y.; Liao, J.; Guo, Z. Distribution of Rare Earth Elements plus Yttrium among Major Mineral Phases of Marine Fe-Mn Crusts from the South China Sea and Western Pacific Ocean: A Comparative Study. *Minerals* **2019**, *9*, 8. [CrossRef]

130. Li, Y.; Huang, G.H.; Zhang, B.Y.; Guo, S.H. Scavenging of Cd through Fe/Mn oxides within natural surface coatings. *J. Environ. Sci.* **2006**, *18*, 1199–1203. [CrossRef]

131. Sun, Q.; Cui, P.-X.; Fan, T.-T.; Wu, S.; Zhu, M.; Alves, M.E.; Zhou, D.-M.; Wang, Y.-J. Effects of Fe(II) on Cd(II) immobilization by Mn(III)-rich δ-MnO$_2$. *Chem. Eng. J.* **2018**, *353*, 167–175. [CrossRef]

132. Kashiwabara, T.; Kubo, S.; Tanaka, M.; Senda, R.; Iizuka, T.; Tanimizu, M.; Takahashi, Y. Stable isotope fractionation of tungsten during adsorption on Fe and Mn (oxyhydr) oxides. *Geochim. Et Cosmochim. Acta* **2017**, *204*, 52–67. [CrossRef]

133. Arai, Y. X-ray Absorption Spectroscopic Investigation of Molybdenum Multinuclear Sorption Mechanism at the Goethite−Water Interface. *Environ. Sci. Technol.* **2010**, *44*, 8491–8496. [CrossRef]

134. Qin, H.; Uesugi, S.; Yang, S.; Tanaka, M.; Kashiwabara, T.; Itai, T.; Usui, A.; Takahashi, Y. Enrichment mechanisms of antimony and arsenic in marine ferromanganese oxides: Insights from the structural similarity. *Geochim. Et Cosmochim. Acta* **2019**, *257*, 110–130. [CrossRef]

135. Yang, K.L.; Zhou, J.S.; Lou, Z.M.; Zhou, X.R.; Liu, Y.L.; Li, Y.Z.; Baig, S.A.; Xu, X.H. Removal of Sb(V) from aqueous solutions using Fe-Mn binary oxides: The influence of iron oxides forms and the role of manganese oxides. *Chem. Eng. J.* **2018**, *354*, 577–588. [CrossRef]

136. Lan, S.; Ying, H.; Wang, X.; Liu, F.; Tan, W.; Huang, Q.; Zhang, J.; Feng, X. Efficient catalytic As(III) oxidation on the surface of ferrihydrite in the presence of aqueous Mn(II). *Water Res.* **2018**, *128*, 92–101. [CrossRef]

137. Bai, Y.H.; Jefferson, W.A.; Liang, J.S.; Yang, T.T.; Qu, J.H. Antimony oxidation and adsorption by in-situ formed biogenic Mn oxide and Fe-Mn oxides. *J. Environ. Sci.* **2017**, *54*, 126–134. [CrossRef]

138. Manning, B.A.; Fendorf, S.E.; Bostick, B.; Suarez, D.L. Arsenic(III) oxidation and arsenic(V) adsorption reactions on synthetic birnessite. *Environ. Sci. Technol.* **2002**, *36*, 976–981. [CrossRef]

139. Zhang, G.S.; Qu, J.H.; Liu, H.J.; Liu, R.P.; Li, G.T. Removal mechanism of As(III) by a novel Fe-Mn binary oxide adsorbent: Oxidation and sorption. *Environ. Sci. Technol.* **2007**, *41*, 4613–4619. [CrossRef]

140. Leuz, A.-K.; Mönch, H.; Johnson, C.A. Sorption of Sb(III) and Sb(V) to Goethite: Influence on Sb(III) Oxidation and Mobilization. *Environ. Sci. Technol.* **2006**, *40*, 7277–7282. [CrossRef]

141. Lafferty, B.J.; Ginder-Vogel, M.; Zhu, M.; Livi, K.J.T.; Sparks, D.L. Arsenite Oxidation by a Poorly Crystalline Manganese-Oxide. 2. Results from X-ray Absorption Spectroscopy and X-ray Diffraction. *Environ. Sci. Technol.* **2010**, *44*, 8467–8472. [CrossRef] [PubMed]

142. Zhang, G.S.; Liu, F.D.; Liu, H.J.; Qu, J.H.; Liu, R.P. Respective Role of Fe and Mn Oxide Contents for Arsenic Sorption in Iron and Manganese Binary Oxide: An X-ray Absorption Spectroscopy Investigation. *Environ. Sci. Technol.* **2014**, *48*, 10316–10322. [CrossRef]

143. Tokoro, C.; Yatsugi, Y.; Koga, H.; Owada, S. Sorption Mechanisms of Arsenate during Coprecipitation with Ferrihydrite in Aqueous Solution. *Environ. Sci. Technol.* **2010**, *44*, 638–643. [CrossRef]

144. Takematsu, N.; Sato, Y.; Okabe, S.; Usui, A. Uptake of selenium and other oxyanionic elements in marine ferromanganese concretions of different origins. *Mar. Chem.* **1990**, *31*, 271–283. [CrossRef]

145. Balistrieri, L.S.; Chao, T.T. Adsorption of selenium by amorphous iron oxyhydroxide and manganese-dioxide. *Geochim. Et Cosmochim. Acta* **1990**, *54*, 739–751. [CrossRef]

146. Wu, Z.; Lanson, B.; Feng, X.; Yin, H.; Tan, W.; He, F.; Liu, F. Transformation of the phyllomanganate vernadite to tectomanganates with small tunnel sizes: Favorable geochemical conditions and fate of associated Co. *Geochim. Et Cosmochim. Acta* **2021**, *295*, 224–236. [CrossRef]

147. Wang, Z.; Kwon, K.D.; Peacock, C.; Mo, X.X.; Gou, W.X.; Feng, X.H.; Li, W. Zn stable isotope fractionation during adsorption onto todorokite: A molecular perspective from X-ray absorption spectroscopy and density functional theory. *Geochim. Et Cosmochim. Acta* **2022**, *327*, 116–136. [CrossRef]

148. Marchig, V.; Vonstackelberg, U.; Hufnagel, H.; Durn, G. Compositional changes of surface sediments and variability of manganese nodules in the Peru Basin. *Deep. Sea Res. Part II Top. Stud. Oceanogr.* **2001**, *48*, 3523–3547. [CrossRef]

149. Manceau, A.; Steinmann, S.N. Density Functional Theory Modeling of the Oxidation Mechanism of Co(II) by Birnessite. *ACS Earth Space Chem.* **2022**, *6*, 2063–2075. [CrossRef]

150. Manceau, A.; Lanson, M.; Geoffroy, N. Natural speciation of Ni, Zn, Ba, and As in ferromanganese coatings on quartz using X-ray fluorescence, absorption, and diffraction. *Geochim. Et Cosmochim. Acta* **2007**, *71*, 95–128. [CrossRef]

151. Manceau, A.; Schlegel, M.L.; Musso, M.; Sole, V.A.; Gauthier, C.; Petit, P.E.; Trolard, F. Crystal chemistry of trace elements in natural and synthetic goethite. *Geochim. Et Cosmochim. Acta* **2000**, *64*, 3643–3661. [CrossRef]

152. Li, D.; Fu, Y.; Sun, X.; Wei, Z. Critical metal enrichment mechanism of deep-sea hydrogenetic nodules: Insights from mineralogy and element mobility. *Ore Geol. Rev.* **2020**, *118*, 103371. [CrossRef]

153. Peacock, C.L. Physiochemical controls on the crystal-chemistry of Ni in birnessite: Genetic implications for ferromanganese precipitates. *Geochim. Et Cosmochim. Acta* **2009**, *73*, 3568–3578. [CrossRef]

154. Peacock, C.L.; Sherman, D.M. Sorption of Ni by birnessite: Equilibrium controls on Ni in seawater. *Chem. Geol.* **2007**, *238*, 94–106. [CrossRef]

155. Sorensen, J.V.; Gueguen, B.; Stewart, B.D.; Pena, J.; Rouxel, O.; Toner, B.M. Large nickel isotope fractionation caused by surface complexation reactions with hexagonal birnessite. *Chem. Geol.* **2020**, *537*, 119481. [CrossRef]

156. Little, S.H.; Sherman, D.M.; Vance, D.; Hein, J.R. Molecular controls on Cu and Zn isotopic fractionation in Fe-Mn crusts. *Earth Planet. Sci. Lett.* **2014**, *396*, 213–222. [CrossRef]

157. Peacock, C.L.; Sherman, D.M. Copper(II) sorption onto goethite, hematite and lepidocrocite: A surface complexation model based on ab initio molecular geometries and EXAFS spectroscopy1 1Associate editor: D. L. Sparks. *Geochim. Et Cosmochim. Acta* **2004**, *68*, 2623–2637. [CrossRef]

158. Shi, D.D.; Wang, S.Z.; Li, Y.; Di, Y.W.; Wang, T. The adsorption mechanism of Zn^{2+} by triclinic birnessite and the mechanism. *Environ. Technol.* **2022**, *43*, 927–934. [CrossRef] [PubMed]

159. Zhao, S.L.; Wang, Q.; Sun, J.Y.; Borkiewicz, O.J.; Huang, R.X.; Saad, E.M.; Fields, B.; Chen, S.; Zhu, M.Q.; Tang, Y.Z. Effect of Zn coprecipitation on the structure of layered Mn oxides. *Chem. Geol.* **2018**, *493*, 234–245. [CrossRef]

160. Yin, H.; Wang, X.; Qin, Z.; Ginder-Vogel, M.; Zhang, S.; Jiang, S.; Liu, F.; Li, S.; Zhang, J.; Wang, Y. Coordination geometry of Zn^{2+} on hexagonal turbostratic birnessites with different Mn average oxidation states and its stability under acid dissolution. *J. Environ. Sci.* **2018**, *65*, 282–292. [CrossRef] [PubMed]

161. Byrne, R.H.; Sholkovitz, E.R. Chapter 158 Marine chemistry and geochemistry of the lanthanides. In *Handbook on the Physics and Chemistry of Rare Earths*; Elsevier: Hoboken, NJ, USA, 1996; Volume 23, pp. 497–593.

162. Aplin, A.C. Rare-earth element geochemistry of central pacific ferromanganese encrustations. *Earth Planet. Sci. Lett.* **1984**, *71*, 13–22. [CrossRef]

163. Bau, M. Scavenging of dissolved yttrium and rare earths by precipitating iron oxyhydroxide: Experimental evidence for Ce oxidation, Y-Ho fractionation, and lanthanide tetrad effect. *Geochim. Et Cosmochim. Acta* **1999**, *63*, 67–77. [CrossRef]

164. Byrne, R.H.; Kim, K.-H. Rare earth element scavenging in seawater. *Geochim. Et Cosmochim. Acta* **1990**, *54*, 2645–2656. [CrossRef]

165. Koeppenkastrop, D.; De Carlo, E.H. Sorption of rare-earth elements from seawater onto synthetic mineral particles: An experimental approach. *Chem. Geol.* **1992**, *95*, 251–263. [CrossRef]

166. Bau, M.; Koschinsky, A. Oxidative scavenging of cerium on hydrous Fe oxide: Evidence from the distribution of rare earth elements and yttrium between Fe oxides and Mn oxides in hydrogenetic ferromanganese crusts. *Geochem. J.* **2009**, *43*, 37–47. [CrossRef]

167. Deng, Y.; Ren, J.; Guo, Q.; Cao, J.; Wang, H.; Liu, C. Rare earth element geochemistry characteristics of seawater and porewater from deep sea in western Pacific. *Sci. Rep.* **2017**, *7*, 16539. [CrossRef]

168. Khanchuk, A.I.; Mikhailik, P.E.; Mikhailik, E.V.; Zarubina, N.V.; Blokhin, M.G. Peculiarities of the distribution of rare-earth elements and yttrium in mineral phases of the ferromanganese crusts from the Detroit guyot (Pacific Ocean). *Dokl. Earth Sci.* **2015**, *465*, 1243–1247. [CrossRef]

169. De Carlo, E.H.; Wen, X.-Y. The Influence of Redox Reactions on the Uptake of Dissolved Ce by Suspended Fe and Mn Oxide Particles. *Aquat. Geochem.* **1997**, *3*, 357–389. [CrossRef]

170. Nakada, R.; Takahashi, Y.; Tanimizu, M. Cerium stable isotope ratios in ferromanganese deposits and their potential as a paleo-redox proxy. *Geochim. Et Cosmochim. Acta* **2016**, *181*, 89–100. [CrossRef]

171. Ohta, A.; Kawabe, I. Rare earth element partitioning between Fe oxyhydroxide precipitates and aqueous NaCl solutions doped with NaHCO3: Determinations of rare earth element complexation constants with carbonate ions. *Geochem. J.* **2000**, *34*, 439–454. [CrossRef]

172. Quinn, K.A.; Byrne, R.H.; Schijf, J. Comparative Scavenging of Yttrium and the Rare Earth Elements in Seawater: Competitive Influences of Solution and Surface Chemistry. *Aquat. Geochem.* **2004**, *10*, 59–80. [CrossRef]

173. Goldberg, E.D. Heavy metal analyses in the marine environment—Approaches to quality control. *Mar. Chem.* **1987**, *22*, 117–124. [CrossRef]

174. Sharma, M. Platinum Group Elements and Their Isotopes in the Ocean. In *Encyclopedia of Ocean Sciences*, 3rd ed.; Cochran, J.K., Bokuniewicz, H.J., Yager, P.L., Eds.; Academic Press: Oxford, UK, 2019; pp. 174–180.

175. Banakar, V.K.; Hein, J.R.; Rajan, R.P.; Chodankar, A.R. Platinum group elements and gold in ferromanganese crusts from Afanasiy-Nikitin seamount, equatorial Indian Ocean: Sources and fractionation. *J. Earth Syst. Sci.* **2007**, *116*, 3–13. [CrossRef]

176. Baturin, G.N.; Konopleva, E.V.; Dubinchuk, V.T.; Mel'nikov, M.E. Platinum and gold in the ferromanganese crusts of the Pacific Ocean. *Oceanology* **2005**, *45*, 269–276.

177. Asavin, A.M.; Anikeev, L.I.; Kazakov, V.A.; Andreev, S.I.; Sapozhnikov, D.A.; Roshchina, I.A.; Kogarko, L.N. Trace element and PGE distribution in layered ferromanganese crusts. *Geochem. Int.* **2008**, *46*, 1179–1205. [CrossRef]

178. Berezhnaya, E.D.; Dubinin, A.V.; Rimskaya-Korsakova, M.N.; Safin, T.H. Accumulation of Platinum Group Elements in Hydrogenous Fe-Mn Crust and Nodules from the Southern Atlantic Ocean. *Minerals* **2018**, *8*, 275. [CrossRef]

179. Qiu, Z.; Dong, Y.; Ma, W.; Zhang, W.; Yang, K.; Zhao, H. Geochemical characteristics of platinum-group elements in polymetallic nodules from the Northwest Pacific Ocean. *Acta Oceanol. Sin.* **2020**, *39*, 34–42. [CrossRef]

180. Berezhnaya, E.D.; Dubinin, A.V.; Mikhailik, E.V. Platinum Group Elements in Ferromanganese Crusts of the Atlantic Ocean: Forms and Sources of Matter. *Oceanology* **2021**, *61*, 390–403. [CrossRef]

181. Halbach, P.; Puteanus, D.; Manheim, F.T. Platinum concentrations in ferromanganese seamount crusts from the central pacific. *Naturwissenschaften* **1984**, *71*, 577–579. [CrossRef]

182. Cobelo-García, A.; López-Sánchez, D.E.; Almécija, C.; Santos-Echeandía, J. Behavior of platinum during estuarine mixing (Pontevedra Ria, NW Iberian Peninsula). *Mar. Chem.* **2013**, *150*, 11–18. [CrossRef]

183. Li, Z.; Sun, X.; Li, D.; Liang, Y.; Li, S.; Peng, J. Platinum enrichment in marine ferromanganese oxides: Constraints from surface adsorption behavior on synthetic feroxyhyte (δ-FeOOH). *Chem. Geol.* **2023**, *615*, 121204. [CrossRef]

184. Boyle, E.A.; Sclater, F.; Edmond, J.M. On the marine geochemistry of cadmium. *Nature* **1976**, *263*, 42–44. [CrossRef]

185. Lee, D.S.; Edmond, J.M. Tellurium species in seawater. *Nature* **1985**, *313*, 782–785. [CrossRef]

186. Biver, M.; Quentel, F.; Filella, M. Direct determination of tellurium and its redox speciation at the low nanogram level in natural waters by catalytic cathodic stripping voltammetry. *Talanta* **2015**, *144*, 1007–1013. [CrossRef]

187. Harada, T.; Takahashi, Y. Origin of the difference in the distribution behavior of tellurium and selenium in a soil–water system. *Geochim. Et Cosmochim. Acta* **2008**, *72*, 1281–1294. [CrossRef]

188. Fukami, Y.; Kashiwabara, T.; Amakawa, H.; Shibuya, T.; Usui, A.; Suzuki, K. Tellurium stable isotope composition in the surface layer of ferromanganese crusts from two seamounts in the Northwest Pacific Ocean. *Geochim. Et Cosmochim. Acta* **2022**, *318*, 279–291. [CrossRef]

189. Baturin, G.N.; Dubinchuk, V.T.; Azarnova, L.A.; Mel'nikov, M.E. Species of molybdenum, thallium, and tellurium in ferromanganese crusts of oceanic Seamounts. *Oceanology* **2007**, *47*, 415–422. [CrossRef]

190. Peacock, C.L.; Moon, E.M. Oxidative scavenging of thallium by birnessite: Explanation for thallium enrichment and stable isotope fractionation in marine ferromanganese precipitates. *Geochim. Et Cosmochim. Acta* **2012**, *84*, 297–313. [CrossRef]

191. Cutter, G.A.; Cutter, L.S. Sources and cycling of selenium in the western and equatorial Atlantic Ocean. *Deep.-Sea Res. Part Ii-Top. Stud. Oceanogr.* **2001**, *48*, 2917–2931. [CrossRef]

192. Swedlund, P.J.; Webster, J.G.; Miskelly, G.M. Goethite adsorption of Cu(II), Pb(II), Cd(II), and Zn(II) in the presence of sulfate: Properties of the ternary complex. *Geochim. Et Cosmochim. Acta* **2009**, *73*, 1548–1562. [CrossRef]

193. Wang, Y.; Feng, X.; Villalobos, M.; Tan, W.; Liu, F. Sorption behavior of heavy metals on birnessite: Relationship with its Mn average oxidation state and implications for types of sorption sites. *Chem. Geol.* **2012**, *292–293*, 25–34. [CrossRef]

194. Zhou, Q.W.; Liao, B.H.; Lin, L.N.; Qiu, W.W.; Song, Z.G. Adsorption of Cu(II) and Cd(II) from aqueous solutions by ferromanganese binary oxide-biochar composites. *Sci. Total Environ.* **2018**, *615*, 115–122. [CrossRef]

195. Schmitt, A.-D.; Galer, S.J.G.; Abouchami, W. Mass-dependent cadmium isotopic variations in nature with emphasis on the marine environment. *Earth Planet. Sci. Lett.* **2009**, *277*, 262–272. [CrossRef]

196. Randall, S.R.; Sherman, D.M.; Ragnarsdottir, K.V. An extended X-ray absorption fine structure spectroscopy investigation of cadmium sorption on cryptomelane (KMn_8O_{16}). *Chem. Geol.* **1998**, *151*, 95–106. [CrossRef]

197. Stoffynegli, P.; Mackenzie, F.T. Mass balance of dissolved lithium in the oceans. *Geochim. Et Cosmochim. Acta* **1984**, *48*, 859–872. [CrossRef]

198. Rajani, P.R.; Manoj, R.V.; Joshi, R.K.; Jishnu, B.K.; Nagasundaram, M. Base metals- and Lithium- rich ferromanganese oxide deposits from the South Andaman Sea, Northeastern Indian Ocean: Mode of occurrence and genesis. *J. Asian Earth Sci.* **2022**, *234*, 105272. [CrossRef]

199. Chan, L.-H.; Hein, J.R. Lithium contents and isotopic compositions of ferromanganese deposits from the global ocean. *Deep. Sea Res. Part II Top. Stud. Oceanogr.* **2007**, *54*, 1147–1162. [CrossRef]

200. Feng, Q.; Yanagisawa, K.; Yamasaki, N. Synthesis of Birnessite-Type Lithium Manganese Oxide. *J. Ceram. Soc. Jpn.* **1996**, *104*, 897–899. [CrossRef]

201. Sohrin, Y.; Isshiki, K.; Kuwamoto, T.; Nakayama, E. Tungsten in north pacific waters. *Mar. Chem.* **1987**, *22*, 95–103. [CrossRef]

202. Kashiwabara, T.; Takahashi, Y.; Tanimizu, M.; Usui, A. Molecular-scale mechanisms of distribution and isotopic fractionation of molybdenum between seawater and ferromanganese oxides. *Geochim. Et Cosmochim. Acta* **2011**, *75*, 5762–5784. [CrossRef]

203. Peacock, C.L.; Sherman, D.M. Vanadium(V) adsorption onto goethite (α-FeOOH) at pH 1.5 to 12: A surface complexation model based on ab initio molecular geometries and EXAFS spectroscopy. *Geochim. Et Cosmochim. Acta* **2004**, *68*, 1723–1733. [CrossRef]

204. Wang, X.Y.; Sherman, D.M. Molecular speciation of Mo (VI) on goethite and its implications for molybdenum and its isotopic cycle in ocean. *Geochim. Et Cosmochim. Acta* **2021**, *313*, 116–132. [CrossRef]

205. Gustafsson, J.P.; Tiberg, C. Molybdenum binding to soil constituents in acid soils: An XAS and modelling study. *Chem. Geol.* **2015**, *417*, 279–288. [CrossRef]

206. Naeem, A.; Westerhoff, P.; Mustafa, S. Vanadium removal by metal (hydr)oxide adsorbents. *Water Res.* **2007**, *41*, 1596–1602. [CrossRef]

207. Ren, Y.Z.; Guan, Y.; Sun, X.M.; Xu, L.; Xiao, Z.L.; Deng, Y.Q.; He, W.T. Nano-mineralogy and growth environment of Fe-Mn polymetallic crusts and nodules from the South China Sea. *Front. Mar. Sci.* **2023**, *10*, 1141926. [CrossRef]

208. Jiang, X.; Yao, D.; Lin, X.; Zhai, S. Geochemistry of Cu, Co, Ni, Ti, and Mg in diagenetic ferromanganese nodules. *Mar. Geol. Quat. Geol.* **2007**, *27*, 47–54.

209. Filella, M.; Belzile, N.; Chen, Y.W. Antimony in the environment: A review focused on natural waters I. Occurrence. *Earth-Sci. Rev.* **2002**, *57*, 125–176. [CrossRef]

210. Sun, Q.; Liu, C.; Alves, M.E.; Ata-Ul-Karim, S.T.; Zhou, D.-M.; He, J.-Z.; Cui, P.-X.; Wang, Y.-J. The oxidation and sorption mechanism of Sb on δ-MnO_2. *Chem. Eng. J.* **2018**, *342*, 429–437. [CrossRef]

211. Marcus, M.A.; Manceau, A.; Kersten, M. Mn, Fe, Zn and As speciation in a fast-growing ferromanganese marine nodule. *Geochim. Et Cosmochim. Acta* **2004**, *68*, 3125–3136. [CrossRef]

212. Kashiwabara, T.; Mitsunobu, S.; Das, A.; Itai, T.; Tanimizu, M.; Takahashi, Y. Oxidation states of antimony and arsenic in marine ferromanganese oxides related to their fractionation in oxic marine environment. *Chem. Lett.* **2008**, *37*, 756–757. [CrossRef]

213. Manceau, A. The mechanism of anion adsorption on iron-oxides—Evidence for the bonding of arsenate tetrahedra on free $Fe(O,OH)_6$ edges. *Geochim. Et Cosmochim. Acta* **1995**, *59*, 3647–3653. [CrossRef]

214. Villalobos, M.; Escobar-Quiroz, I.N.; Salazar-Camacho, C. The influence of particle size and structure on the sorption and oxidation behavior of birnessite: I. Adsorption of As(V) and oxidation of As(III). *Geochim. Et Cosmochim. Acta* **2014**, *125*, 564–581. [CrossRef]

215. Wang, S.L.; Mulligan, C.N. Speciation and surface structure of inorganic arsenic in solid phases: A review. *Environ. Int.* **2008**, *34*, 867–879. [CrossRef]